

1 **In situ measurements of cloud microphysics and aerosol over**
2 **coastal Antarctica during the MAC campaign**

3

4 **Sebastian J. O'Shea¹, Thomas W. Choularton¹, Michael Flynn¹, Keith N. Bower¹,**
5 **Martin Gallagher¹, Jonathan Crosier^{1,2}, Ian Crawford³, Zoë L. Fleming⁴, Constantino**
6 **Listowski^{4*}, Amélie Kirchgaessner⁴, Russell S. Ladkin⁴, and Thomas Lachlan-Cope⁴**

7

8 [1]{School of Earth and Environmental Sciences, University of Manchester, Oxford Road,
9 Manchester, M13 9PL, UK}

10 [2]{National Centre for Atmospheric Science, University of Manchester, Oxford Road,
11 Manchester, M13 9PL, UK}

12 [3]{National Centre for Atmospheric Science, Department of Chemistry, University of
13 Leicester, Leicester, LE1 7RH, UK}

14 [4]{British Antarctic Survey, NERC, High Cross, Madingley Rd, Cambridge CB3 0ET, UK}

15 *now at: LATMOS/IPSL, UVSQ Université Paris-Saclay, UPMC Univ. Paris 06, CNRS,
16 Guyancourt, France

17 Correspondence to: S. J. O'Shea (sebastian.oshea@manchester.ac.uk)

18

19 **Abstract**

20 During austral summer 2015 the Microphysics of Antarctic Clouds (MAC) field campaign
21 collected unique and detailed airborne and ground based in situ measurements of cloud and
22 aerosol properties over coastal Antarctica and the Weddell Sea. This paper presents the first
23 results from the experiment and discusses the key processes important in this region, which is
24 critical to predicting future climate change

25 The sampling was predominantly of stratus cloud, at temperatures between -20 and 0 °C.
26 These clouds were dominated by supercooled liquid water droplets, which had a median
27 concentration of 113 cm⁻³ and an inter-quartile range of 86 cm⁻³. Both cloud liquid water

1 content and effective radius increased closer to cloud top. The cloud drop effective radius
2 increased from $4 \pm 2 \mu\text{m}$ near cloud base to $8 \pm 3 \mu\text{m}$ near cloud top.

3 Cloud ice particle concentrations were highly variable with the ice tending to occur in small
4 isolated patches. Below approximately 2000 m glaciated cloud regions were more common at
5 higher temperatures; however the clouds were still predominantly liquid throughout. When
6 ice was present at temperatures higher than $-10 \text{ }^\circ\text{C}$, secondary ice production most likely
7 through the Hallet-Mossop mechanism lead to ice concentrations 1 to 3 orders of magnitude
8 higher than the number predicted by commonly used primary ice nucleation
9 parameterisations. The drivers of the ice crystal variability are investigated. No clear
10 dependence on the droplet size distribution was found. The source of first ice in the clouds
11 remains uncertain, but may include contributions from biogenic particles, blowing snow or
12 other surface ice production mechanisms.

13 The concentration of large aerosols (diameters 0.5 to 1.6 μm) decreased with altitude and
14 were depleted in airmasses that originated over the Antarctic Continent compared to those
15 more heavily influenced by the Southern Ocean and sea ice regions. The dominant aerosol in
16 the region was hygroscopic in nature, with the hygroscopicity parameter, κ having a median
17 value for the campaign of 0.64 (interquartile range = 0.34). This is consistent with other
18 remote marine locations that are dominated by sea salt/sulphate.

19

20 **1 Introduction**

21 Antarctic clouds have a central role in the weather and climate at high southern latitudes
22 (Lubin et al., 1998; Lawson and Gettelman, 2014). Through snow precipitation and their
23 radiative effects they are key to the mass balance of the Antarctic ice sheet, which impacts on
24 global sea levels (van den Broeke et al., 2011) and Southern Ocean circulation (Bromwich et
25 al., 2012). In addition it has been suggested that changes in Antarctic clouds can influence
26 weather patterns as far away as the tropics and even the extratropics of the Northern
27 Hemisphere (Lubin et al., 1998).

28 Despite their importance Antarctic clouds are some of the least studied of any region around
29 the globe (Bromwich et al., 2012). The remote location and harsh conditions cause significant
30 logistical challenges for field projects in this region. As a consequence there is evidence that
31 clouds and their radiative properties are poorly represented in weather and climate models

1 over Antarctica (Bromwich et al., 2013; King et al., 2015; Listowski and Lachlan-Cope,
2 2017) and the Southern Ocean (Bodas-Salcedo et al., 2012; 2016).

3 Key uncertainties concern the aerosol in the region, in particular the number and sources of
4 cloud condensation nuclei (CCN) and ice nucleating particles (INPs). Conventional
5 parameterisations predicting INP concentrations have primarily been developed using
6 measurements at mid-latitudes (e.g. Cooper, 1986; DeMott et al., 2010) and may not be
7 appropriate for Antarctica. A number of intensive field campaigns have been conducted
8 studying Arctic clouds (McFarquhar and Cober, 2004; McFarquhar et al., 2007; Verlinde et
9 al., 2007; Lloyd et al., 2015a), however analogies between the polar regions may also not be
10 appropriate. The Arctic receives significant anthropogenic aerosol input due to its proximity
11 to industrial nations, and is therefore likely to have significantly different type and number of
12 CCN/INP (Mauritsen et al., 2011; Latham et al., 2013; Liu et al., 2015).

13 Previous, multi-year measurements of aerosol at the Neumayer coastal Antarctic research
14 station had a median concentration of 258 cm^{-3} . Minimum values (less than 100 cm^{-3}) were
15 typically observed in June/July, while concentrations increased in the austral summer to a
16 maximum of approximately 1000 cm^{-3} in March (Weller et al., 2011). In winter, aerosol
17 number and mass were both dominated by sea salt particles (87% by mass, Weller et al.,
18 2008). Although aerosol composition in summer is more variable, sea salt still accounts for a
19 significant fraction (50% by mass) but now with a large contribution from non-sea salt
20 sulphate (27% by mass, Weller et al., 2008). Measurements at the coastal Antarctic station
21 McMurdo show the persistent presence of sulphate aerosol throughout the year (Giordano et
22 al., 2017). In the winter these particles are highly aged. Sulphate aerosol then increases
23 through the austral spring/summer, due to enhanced emissions of dimethyl sulphide (DMS)
24 and methanesulfonic acid (MSA) from phytoplankton in the Southern Ocean (Gibson et al.,
25 1990; Giordano et al., 2017). Giordano et al. (2017) also report the presence of a sub-250 nm
26 aerosol population of unknown composition during the winter to summer transition. In
27 addition a study has observed a significant fraction of organic carbon (>10%) and lower
28 contributions from sea salt (<10%) in summer marine Antarctic aerosol (Virkkula and Teinil,
29 2006). Measurements in the Antarctic have found that the aerosol is highly hygroscopic in
30 marine airmasses (Mangold et al., 2017). While continental aerosol is less hygroscopic, which
31 is consistent with a lower MSA fraction and the aging of marine organic components (Asmi et
32 al., 2010). To date, Antarctic INP measurements have mostly been made at surface sites.

1 Measurements of snowflake residuals at the South Pole identified the long range transport of
2 clays as the likely dominant source (Kumai, 1976). However, interpretation of these
3 measurements is complicated due to secondary aerosol scavenging by the snowflakes and
4 precipitation, meaning they contain particles in addition to the original nuclei. More recently,
5 filter samples at the South Pole detected INPs that were active between -18 and -27°C, with
6 concentrations of 1 L^{-1} at -23 °C. Mineral dusts transported from the Patagonian deserts were
7 identified as the likely source (Ardon-Dryer et al., 2011). A synthesis of INP measurements
8 prior to 1988 from the high southern latitudes ($> 60^\circ\text{S}$), found mean concentrations between
9 2×10^{-4} and 0.2 L^{-1} at -15°C (Bigg, 1990). Given the general absence of other local INP
10 sources, biogenic INPs may have a more important role in the Antarctic than in other regions.
11 Biological species (pollen, bacteria, fungal spores and plankton) have been shown to act as
12 INP at significantly higher temperatures than mineral dusts ($> -15^\circ\text{C}$) (Möhler et al., 2007;
13 Alpert et al., 2011; Murray et al., 2012; Amato et al., 2015; Wilson et al., 2015). However,
14 Antarctic snowfall has been shown to be relatively depleted of biological INP (Christner et
15 al., 2008) and bacteria commonly found in sea ice may not be effective INP (Junge and
16 Swanson, 2007). The few in situ measurements of Antarctic clouds to date have suggested the
17 importance of secondary ice processes (Grosvenor et al., 2012; Lachlan-Cope et al., 2016).

18 There is a clear need for more direct measurements to test and improve the representation of
19 Antarctic clouds in climate/weather models. This paper presents both ground based and
20 airborne measurements of cloud and aerosol properties during the 2015 Microphysics of
21 Antarctic Clouds (MAC) field campaign aimed at addressing this. Section 2 provides an
22 overview of the campaign and the measurement techniques used. Section 3 presents a
23 statistical overview of the aerosol and cloud observations using all available measurements.
24 Section 4 discusses the key microphysical processes. Conclusions are presented in Sect. 5.

25

26 **2 Methods**

27 **2.1 Campaign and meteorological overview**

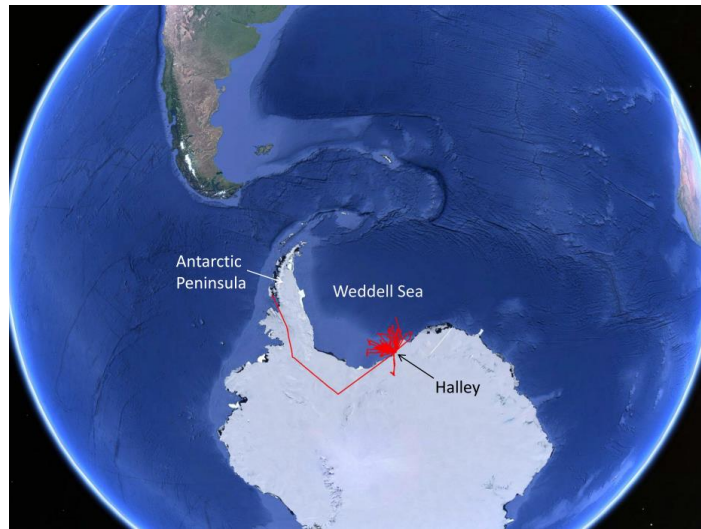
28 The MAC experiment comprised both airborne and ground based measurements of cloud and
29 aerosol properties. Ground based measurements were performed at the Clean Air Sector
30 Laboratory (CASLab), which is located at the Halley research station. Halley is a coastal
31 Antarctic base on the Brunt Ice shelf, approximately 30 km from the Weddell Sea (75.6°S ,

1 26.7° W). The CASLab is located 1 km south of the main Halley buildings and receives
2 minimal pollution from the base and vehicle traffic due to the prevailing easterly wind (Jones
3 et al., 2008). All CASLab measurements were filtered using the wind direction to help
4 remove any remaining influence from the base.

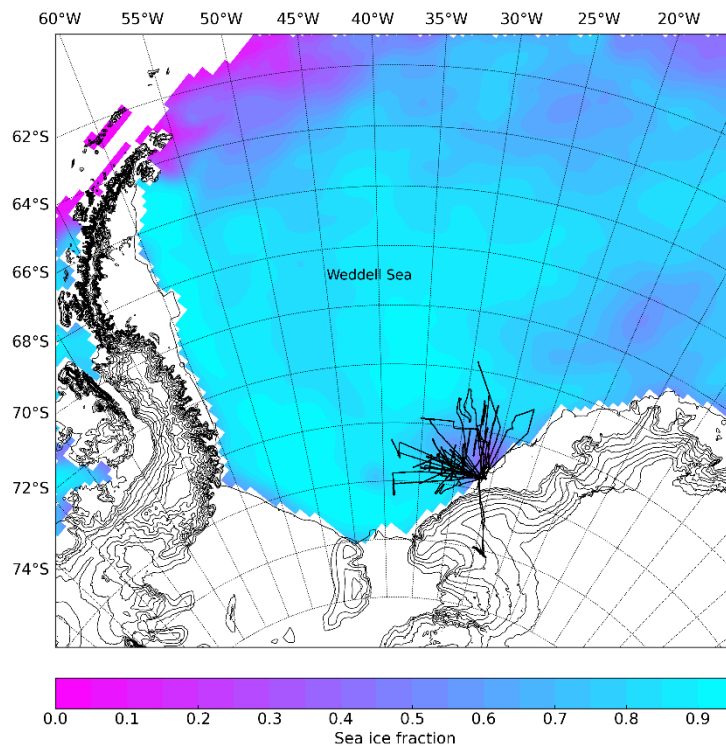
5 The airborne measurements were collected using the British Antarctic Survey's Twin Otter
6 MASIN research aircraft (King et al., 2008). Twenty-four flights (a total of 80 hours) were
7 performed during November and December 2015 from Halley. These flights have the nominal
8 flight numbers 212 to 235. The flights were predominantly performed over the Weddell Sea
9 (see Fig. 1), which at this time and location was covered by a mixture of broken sea ice and
10 polynyas. This is shown in Fig. 1 together with the sea ice fraction (Maslanik and Stroeve,
11 1999). One flight sampled clouds in-land over the Antarctic continent (Flight 233). In
12 addition a transit took place from Rothera research station on the Antarctic Peninsula (Flights
13 212 to 215); however not all instruments were available during these transit flights. Since the
14 aircraft was not pressurised, the measurements were restricted to altitudes below
15 approximately 4000 m. As a consequence, the majority of clouds were sampled over the
16 temperature range -11 and -3 °C (79%). Seventeen percent of in-cloud measurements were
17 collected at temperatures below -11 °C and 4% at temperatures higher than -3 °C. In total 17
18 hours of sampling during the campaign was performed in-cloud.

19

20



1



2

3 *Figure 1. Top panel: Flight tracks during the MAC field project (source Google Earth).*
 4 *Lower panel: shows the sea ice fraction on the Weddell Sea (Maslanik and Stroeve, 1999)*
 5 *during the experimental period.*

6

7 The clouds sampled were generally stratiform, with strong temperature inversions at cloud
 8 top. The exception to this was Flight 224, which sampled frontal clouds. Table 1 shows the

1 altitude and temperature of cloud base/top for each flight. If multiple layers were present,
2 unless otherwise noted, the height and temperatures given are of the layer where the majority
3 of sampling took place. To show the meteorological setting for the campaign Figures S1 to
4 S20 show surface pressure charts from the ERA-Interim reanalysis (at 12 UTC on the given
5 day, Dee et al., 2011) and HYSPLIT (Hybrid Single-Particle Lagrangian Integrated
6 Trajectory, Stein et al., 2015) back trajectories for each flight. Back trajectory analysis
7 showed that two broad regimes were present during the project. The earlier flights (up to
8 Flight 223) generally sampled airmasses that had travelled south over the Southern Ocean and
9 Weddell Sea. Later in the campaign there was a transition to airmasses with greater influence
10 from the Antarctic continent.

| Number | Date | Base altitude (m) | Top altitude (m) | Base temperature (°C) | Top temperature (°C) | Comment |
|--------|------------|-------------------|------------------|-----------------------|----------------------|--|
| 216 | 21/11/2015 | 261 (246-283) | 951 (925-983) | -12.1 | -14.1 | Multiple layers. |
| 217 | 24/11/2015 | 330 (296-366) | 662 (621-700) | -9.8 | -12.3 | Multiple layers. |
| 218 | 27/11/2015 | 312 (298-327) | 554 (539-569) | -4.8 | -6.1 | Main layer with broken layers above. |
| 219 | 27/11/2015 | 375 (316-441) | 870 (847-890) | -4.7 | -7.8 | Single layer. |
| 220 | 28/11/2015 | 1143 (1129-1154) | 1303 (1289-1317) | -12.9 | -13.2 | Single layer. |
| 221 | 29/11/2015 | 157 (124-202) | 530 (499-564) | -6.0 | -6.6 | Single layer with high cloud above (3000 m). |
| 222 | 30/11/2015 | 170 (151-201) | 603 (573-635) | -6.8 | -8.5 | Predominately single layer, partial layer above. |
| 223 | 03/12/2015 | 262 (247-277) | 745 (712-771) | -7.1 | -9.5 | Multiple layers. |
| 224 | 06/12/2015 | 1056 (1022-1090) | 4278 (4253-4300) | -7.6 | -18.9 | Frontal cloud multiple layers. Cloud top not sampled. Height and temperature ranges are for all layers sampled. |
| 225 | 07/12/2015 | 694 (680-718) | 1010 (944-1066) | -5.0 | -5.7 | Single layer with high cloud above (4000 m). |
| 226 | 07/12/2015 | 1273 (1230-1319) | 1866 (1853-1873) | -5.4 | -6.8 | Single layer with high cloud above (4000 m). |
| 227 | 08/12/2015 | 88 (68-107) | 417 (372-455) | -5.8 | -6.9 | Single layer. |

| | | | | | | |
|-----|------------|------------------|------------------|-------|-------|---|
| 228 | 09/12/2015 | 76 (50-122) | 528 (493-567) | -6.7 | -5.9 | Single layer. 2 nd partial layer at 1500m. |
| 229 | 09/12/2015 | | | | | No cloud sampled. |
| 230 | 10/12/2015 | 334 (304-362) | 574 (558-588) | -4.6 | -6.5 | Single layer. |
| 231 | 11/12/2015 | 293 (279-321) | 1171 (1158-1186) | -4.6 | -8.3 | Predominantly single layer, partial layer above. |
| 232 | 11/12/2015 | 554 (516-601) | 1126 (1108-1148) | -6.3 | -10.1 | Single layer with high cloud above. |
| 233 | 12/12/2015 | 1630 (1600-1667) | 1857 (1852-1861) | -14.1 | -15.4 | Single broken layer. |
| 234 | 13/12/2015 | 409 (387-428) | 710 (700-720) | -5.9 | -7.1 | Lower layer. |
| | | 1489 (1479-1499) | 1785 (1764-1804) | -13.6 | -13.7 | Higher layer not directly above lower level. |
| 235 | 14/12/2015 | 954 (929-979) | 1432 (1404-1461) | -9.9 | -13.9 | Main layer sampled with broken layers below. |

1 Table 1. The height and temperature of cloud base and top for each flight. The range of altitudes in brackets are an estimate of the uncertainty
2 in the cloud heights due to a combination of variability in the cloud and incomplete sampling. If multiple layers were present, unless noted
3 otherwise, the height and temperatures given are for the main cloud layer sampled.

4

1

2 **2.2 Aircraft**

3 During MAC the Twin Otter MASIN research aircraft was fitted with a range of in situ
4 aerosol and cloud microphysical instrumentation. Cloud particle size distributions were
5 derived using the images from two optical array probes (OAP): a 2DS (2D-stereo, SPEC Inc.,
6 USA, see Lawson et al., 2006) with a nominal size range of 10 to 1280 μm (10 μm pixel
7 resolution) and a CIP-25 (Cloud Imaging Probe, DMT Inc., USA, Baumgardner et al., 2001)
8 with a size range of 25 to 1600 μm (25 μm pixel resolution). The 2DS was not operated on the
9 flights before Flight 218.

10 Particle size distributions over the size range from 0.5 to 50 μm were recorded using a Cloud
11 Aerosol Spectrometer (CAS, DMT Inc., USA, Baumgardner et al., 2001). The CAS sizing
12 was calibrated by the manufacturer using polystyrene latex (PSL) spheres ($< 2 \mu\text{m}$) and glass
13 beads ($> 2 \mu\text{m}$) (Baumgardner et al., 2014). During MAC the sizing of the CAS's larger bins
14 ($>10 \mu\text{m}$) was also validated using reference glass calibration beads and show little instrument
15 drift (see Fig 2.).

16 The aircraft was also fitted with a Cloud Droplet Probe (CDP-100, DMT Inc.) for observing
17 cloud droplets between 3 and 50 μm (Lance et al., 2010). Following the method detailed by
18 Rosenberg et al. (2012), glass beads were used to determine the CDP's size bin centres and
19 widths. The 2DS and CIP-25 were fitted with anti-shatter tips to minimise ice break-up on
20 their leading edges (Korolev et al., 2011). For full details of the data processing and quality
21 control of the 2DS and CIP-25 measurements see Crosier et al. (2011) and Taylor et al.
22 (2016). It should be noted that in addition to the use of anti-shatter tips, an inter-arrival time
23 algorithm was used to further reduce shattering artefacts on the 2DS and CIP-25 datasets. Ice
24 mass content was determined from the 2DS and CIP-25 images using the Brown and Francis
25 (1995) mass-diameter relationship. Unless stated otherwise all flight data presented has been
26 averaged to 10 second intervals. A linear fit to the number concentrations derived by the CDP
27 and CAS where their size ranges overlap has equation $\text{CDP} = 0.87 \times \text{CAS} + 1.7 \text{ cm}^{-3}$ ($R^2 =$
28 0.83). Similarly, the regression equation for the CIP and 2DS is $\text{CIP} = 0.65 \times \text{2DS} + 0.7 \text{ cm}^{-3}$
29 ($R^2 = 0.34$).

30

1

2 Following Crosier et al. (2011), 2DS and CIP-25 images were classified based on a geometric
3 analysis of their circularity, C :

$$4 \quad C = \frac{P^2}{4\pi A}$$

5 Equation 1

6 where P is the particles perimeter and A is its area. Particles containing less than 50 pixels
7 (equivalent to a diameter of approximately 80 μm for the 2DS and 200 μm for the CIP-25)
8 were not classified since they contain insufficient pixels to accurately determine their shape.
9 Particles with circularity values less than 1.2 were classified as low irregular (LI) and are
10 indicative of liquid drops. Circularity values greater than 1.4 are associated with ice crystals
11 and are classified as high irregular (HI). Visual inspection of the LI and HI images confirmed
12 that they were almost all liquid droplets and ice crystals, respectively. Circularities between
13 1.2 and 1.4 are classified as medium irregular (MI). Interpretation of the MI category with
14 respect to the particle phase is more ambiguous than the other categories. In general, the MI
15 images were of quasi-spherical ice crystals, such as recently frozen drops, however they may
16 also include some poorly imaged liquid drops that should be classified as LI. During MAC the
17 concentration of MI particles was generally significantly less than HI particles. The mean
18 ratio HI:MI for the campaign was 7 (see also Sect. 3.1). This suggests that the HI
19 concentration is likely a good proxy for the ice crystal concentration.

20 Aerosol instrumentation on the aircraft included a GRIMM optical particle counter (GRIMM
21 Model 1.109) capable of detecting aerosol particles over the size range from 0.25 to 32 μm .
22 The GRIMM sampled through a Brechtel Model 1200 isokinetic aerosol inlet with a >95%
23 sampling efficiency for particles in the size range 0.01 μm to 6 μm . Inlet losses only become
24 significant for particles >6 μm and here we only consider the concentration of particles below
25 2 μm . Total aerosol concentrations of particles >10 nm in size were determined using a
26 Condensation Particle Counter (CPC, TSI Inc. Model 3772).

27 The aircraft was also fitted with instrumentation to measure temperature, turbulence,
28 humidity, radiation and surface temperature. See King et al. (2008) for full details.

1 2.3 Ground site measurements

2 Aerosol instrumentation was installed at the CASLab sampling from its central aerosol stack
3 (Jones et al., 2008) for the measurement period from 27 November 2015 to 15 December
4 2015. A Scanning Mobility Particle Sizer (SMPS, TSI) was used to generate a quasi-
5 monodisperse aerosol flow. The SMPS performed 27 discrete steps over the aerosol size
6 range from 30 to 500 nm. Downstream of the SMPS the flow (1 L^{-1}) was split isokinetically
7 between a cloud condensation nuclei counter (CCNc, Droplet Measurement Technology
8 Model CCN-100) and a condensation particle counter (CPC, TSI). The CCN concentration
9 was measured at super saturations of 0.05%, 0.13%, 0.20%, 0.26% and 0.34%. The activated
10 cloud droplet fraction was determined by the ratio of activated particles from the CCN to the
11 total number of particles measured by the CPC. The dry diameter at which 50% of particles
12 were activated (D_{50}) was determined by fitting a sigmoid curve to the activated fraction size
13 spectrum (Whitehead et al., 2016). The total CCN concentration was determined by
14 integrating the concentration of particles larger than D_{50} . The hygroscopicity parameter κ was
15 derived from κ -Köhler theory using the D_{50} and supersaturation values (Petters and
16 Kreidenweis, 2007).

17 The SMPS and CCNc were calibrated at the beginning and end of the campaign (Good et al.,
18 2010). The SMPS was size calibrated using NIST traceable polystyrene latex spheres (PSLs).
19 Ammonium sulphate and sodium chloride were used to calibrate the CCNc supersaturations,
20 by comparing measured values to theoretical ones from the Aerosol Diameter Dependent
21 Equilibrium Model (ADDEM) (Topping et al., 2005).

22 Additional measurements were provided by an Aerodynamic Particle Sizer (TSI Model 3321)
23 which provided aerodynamic particle size concentration measurements over the size range
24 $0.5 < D < 20 \mu\text{m}$ and in the size range $0.3 < D < 20 \mu\text{m}$ from simultaneous aerosol scattering cross
25 section measurements. Total aerosol concentrations ($D > 10 \text{ nm}$) were determined using a
26 Condensation Particle Counter (CPC, TSI Inc. Model 3776).

27 Continuous measurements of airborne bio-fluorescent particle concentrations (primary
28 biological and mixed biological and non-biological) were also made at CASLab using a
29 Wideband Integrated Bioaerosol Spectrometer (WIBS Model Dstl-3). Measurements from
30 this instrument are described in detail in Crawford et al. (2017).

1 **2.4 Numerical Atmospheric Dispersion Modelling Environment (NAME)**

2 To examine how aerosol and cloud properties vary with air mass history we perform back
3 trajectory analysis using the UK Met. Office's NAME model (Numerical Atmospheric
4 Dispersion Modelling Environment) (Jones et al., 2007) using Met Office Unified Model
5 (UM) meteorological fields. Five-day retroplumes were determined by releasing 10000
6 particles in the model at locations coincident with the aircraft's position. Here we examine the
7 relative sensitivity to surface emissions from the following regions; the Antarctic continent,
8 sea ice, Southern Ocean, ice-shelf and South America. The numbers of particles near the
9 surface (0 to 100 m) over each geographic region was summed every 15 minutes as the
10 particles were dispersed five-days backwards in time. For each region, the time integration of
11 particles over the region was divided by the total number of particles appearing in the whole
12 domain to determine fractional contributions (see Fleming et al., 2012). Shape files
13 representing the monthly averaged sea ice extent from Polarview and geographical contour
14 files for the Antarctic plateau, the permanent sea ice (ice shelves and permanent sea ice) and
15 the American continent were used to determine the passageway of the air masses at surface
16 levels sampled by the aircraft. This analysis was repeated for particles released at 60s
17 intervals along the flight track to determine a time series of contributions from each
18 geographic region.

19

20 **3 Results**

21 **3.1 Cloud microphysics**

22 The following section presents a broad overview of the microphysical measurements during
23 the MAC field campaign. For this analysis "in-cloud" measurements were determined as
24 periods when the liquid water content (LWC) was greater than 0.01 g m^{-3} or when particles
25 were detected by the 2DS. Flight 224 is excluded from this bulk analysis since this flight
26 sampled frontal cloud, while the other flights sampled shallow layer cloud. The ice mass
27 fraction (IMF) is calculated as the ratio of the ice mass to the total condensed water. Here the
28 ice mass is taken as the sum of the HI and MI 2DS categories, while the liquid mass is taken
29 as the sum of the CAS droplets ($>3 \mu\text{m}$) and the 2DS LI category. Ice mass fractions of 0 and
30 1 represent fully liquid and glaciated conditions, respectively. Figure 2 (black line) shows the
31 frequency distribution of ice mass fraction based on all 1 Hz measurements in layer clouds

1 sampled during MAC. As can be seen in Fig. 2 the clouds were dominated by liquid water.
2 Ice mass fractions between 0 and 0.1 were observed 90% of the time, while only 6% of cases
3 had values between 0.9 and 1. Figure 3 shows the ice mass fraction as a function of height.
4 For altitudes below ca. 2000 m (all altitudes given are meters above mean sea level) there is a
5 general trend of glaciated conditions becoming more prevalent with decreasing altitude (and
6 increasing temperature). At temperatures higher than -3 °C glaciated conditions (IMF greater
7 than 0.9) were responsible for 15% of observations, compared to 7% at temperatures between
8 -8 and -3 °C. Above 2000m glaciated regions become more frequent with increasing altitude,
9 however this is based on comparatively few observations.

10 Figure 3b, shows ice mass fraction measurements in single layer clouds as a function of the
11 normalised position within the cloud, Z_n .

$$Z_n = \frac{Z - Z_B}{Z_T - Z_B},$$

13 Equation 2

14 where Z is the altitude, Z_B and Z_T are cloud base and cloud top altitude, respectively. We note
15 that there is some uncertainty in determining cloud base/top due to variability in the cloud and
16 also incomplete sampling (this uncertainty is estimated in Table 1). The clouds were
17 dominated by liquid drops throughout, while ice was more prevalent lower in the clouds. The
18 relationship between ice mass fraction (IMF) and Z_n over the range $0 < Z_n < 1$ can be
19 approximated by the equation:

$$IMF = 0.177 + 0.360Z_n + 0.244Z_n^2$$

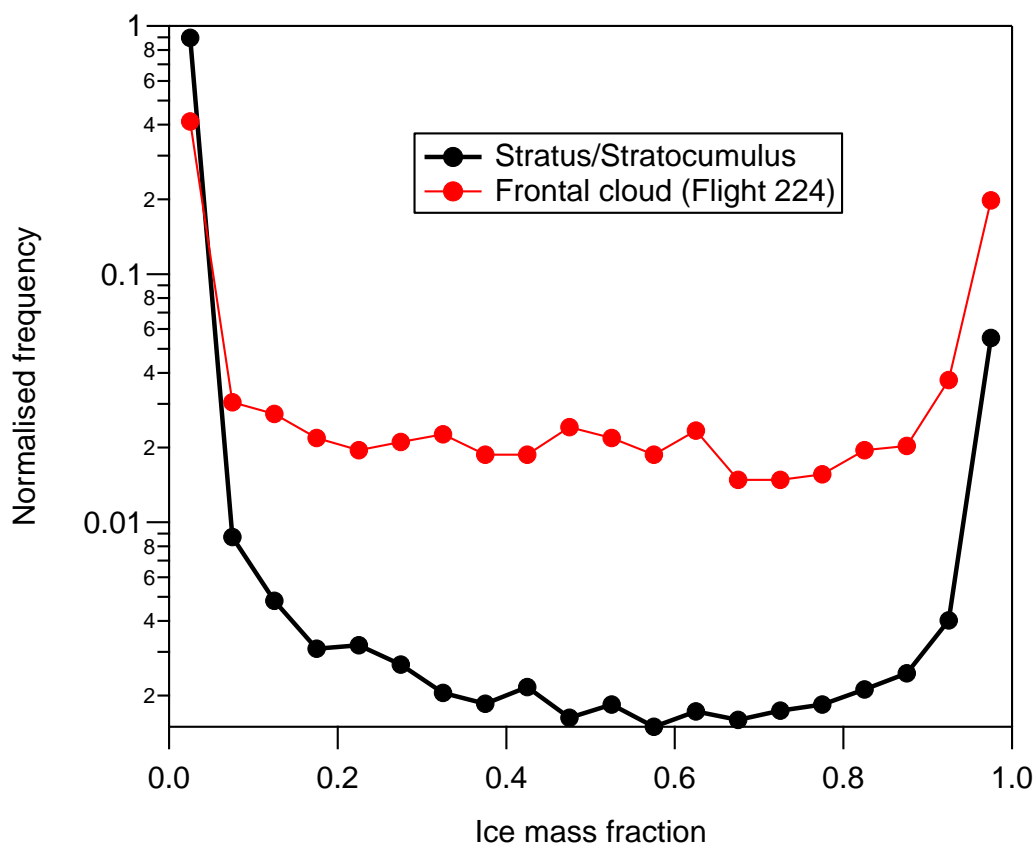
21 Equation 3

22 This is shown as a red line in Fig. 3b. Figure 3c and d show that both liquid water content and
23 cloud drop effective radius increased closer to cloud top. The effective radius increased from
24 $4 \pm 2 \mu\text{m}$ near cloud base to $8 \pm 3 \mu\text{m}$ near cloud top.

25 Measurements in Arctic stratus/stratocumulus generally find these clouds to be similarly
26 dominated by liquid drops (McFarquhar and Cober, 2004; McFarquhar et al., 2007; Lloyd et
27 al., 2015a). A polynomial relationship derived during the Mixed-Phase Arctic Cloud
28 Experiment (M-PACE) is shown as a blue line in Fig. 3b (McFarquhar et al., 2007).
29 McFarquhar et al. (2007) show a trend of increasing IMF with increasing distance from cloud
30 top (and increasing temperature). Glaciated conditions were observed during 23% of their

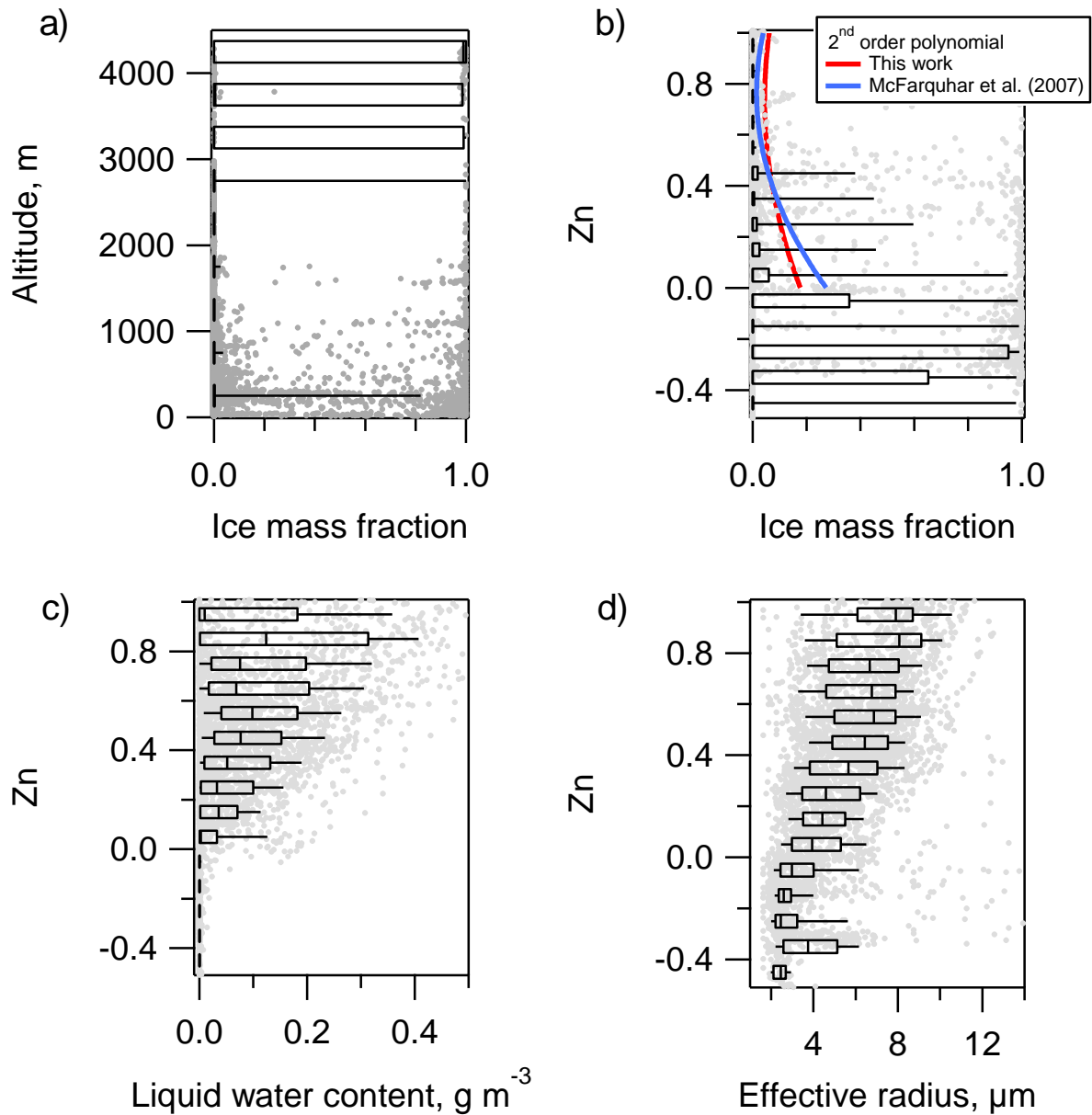
1 measurements. This is significantly more than during MAC, possibly due to lower INP
 2 concentrations available for primary ice development in the Antarctic compared to the Arctic,
 3 but differing sampling strategies may also contribute to this difference.

4 Flight 224 sampled cloud layers at the rear of an occluded front that was associated with a
 5 low pressure system north of Halley. Several layers were observed between $-19\text{ }^{\circ}\text{C}$ and $-1\text{ }^{\circ}\text{C}$
 6 with ice crystals precipitating between the layers. As shown in Fig. 2 (red line) ice was more
 7 frequently observed in these clouds than during the flights where stratocumulus/stratus clouds
 8 were sampled. Twenty-four percent of measurements had ice mass fractions between 0.9 and
 9 1, while 32% of observed ice mass fraction values were between 0.1 and 0.9. Droplet number
 10 concentrations were comparatively low with a mean of 40 (29 at 1σ) cm^{-3} .



11

12 *Figure 2. Frequency distribution of the 1 Hz cloud ice mass fraction measurements.*



1

2 *Figure 3a. Ice mass fraction as a function of altitude and b) normalised position within the*
 3 *cloud (Zn). c) and d) show similar plots for liquid water content and effective radius from the*
 4 *CAS probe. Boxes are the 25th and 75th percentiles, the whiskers are the 10th and 90th*
 5 *percentiles.*

6

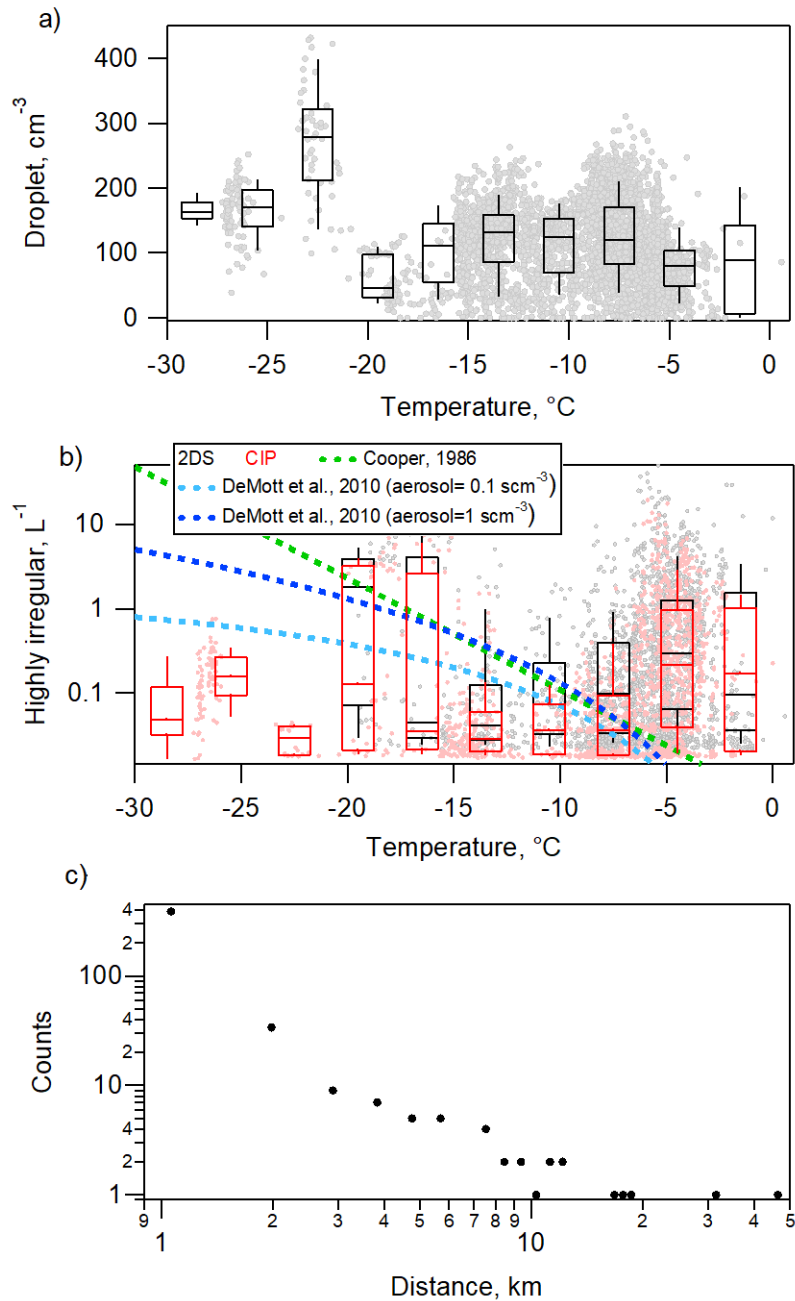
7 The droplet number concentration as a function of temperature is shown in Fig. 4a. This was
 8 found to be relatively consistent and temperature independent during the campaign with a
 9 median of 113 cm^{-3} and an inter-quartile range of 86 cm^{-3} . An exception to this is Flight 217,
 10 when anomalously high droplet concentrations were observed at $-23 \text{ }^\circ\text{C}$ (mean 310 cm^{-3}). The

1 2DS was not available during this flight but the CIP observations suggest that ice was not
2 present in this cloud. The reason for the enhanced droplet concentrations is not clear, however
3 the aerosol concentrations below the cloud layer was similarly elevated with the CPC
4 recording concentrations of over 1200 scm^{-3} , compared to the median for the campaign of 408
5 scm^{-3} . Back trajectory analysis showed that in the previous days this air mass travelled over
6 the Southern Ocean from South America.

7 The cloud droplet concentrations during MAC are found to be comparable with previous
8 observations from the Antarctic Peninsula (Lachlan-Cope et al., 2016) and also Arctic
9 summer stratocumulus (Lloyd et al., 2015a). Droplet concentrations over the Antarctic
10 Peninsula varied between 60 and 200 cm^{-3} (Lachlan-Cope et al., 2016). Concentrations on the
11 eastern side of the Peninsula were moderately higher than on the west, which may be due to
12 the greater sea ice coverage on the eastern side. It has been suggested that sea ice may provide
13 a more efficient source of sea-salt aerosol, and therefore CCN, than open waters (Yang et al.,
14 2008). Recent measurements and modelling found that sea ice made a significant contribution
15 to the winter sea-salt aerosol loading at coastal (Dumont d'Urville) and central (Concordia)
16 East Antarctic sites (Legrand et al., 2016).

17 The number of highly irregular particles observed by the 2DS/ CIP-25 can be used as a proxy
18 for the number of ice crystals; this is shown as a function of temperature in Fig. 4b. Box and
19 whisker plots show statistics for those regions of the cloud where ice is present (i.e. excluding
20 regions with only liquid cloud water). The temperature bins -21 to $-15 \text{ }^\circ\text{C}$ in Fig. 4b show the
21 highest concentration of ice crystals. However these measurements come from only one flight
22 (Flight 226) where the base (4000 m) of high cloud was sampled. These crystals
23 (predominantly rosettes and aggregates) are highly likely to have been nucleated at lower
24 temperatures higher up in the cloud which then sedimented down to be sampled by the
25 aircraft. At temperatures greater than $-15 \text{ }^\circ\text{C}$ there is a trend of the ice crystal concentrations
26 showing greater variability and higher median concentrations with increasing temperature. Ice
27 in the clouds tended to occur in small patches. A histogram of the spatial extent of ice patches
28 shows that they increase in frequency with decreasing length up to the maximum resolvable
29 by the 2DS measurements (a sampling frequency of 10s corresponds to a spatial scale of
30 about 600m , Figure 4c).

31



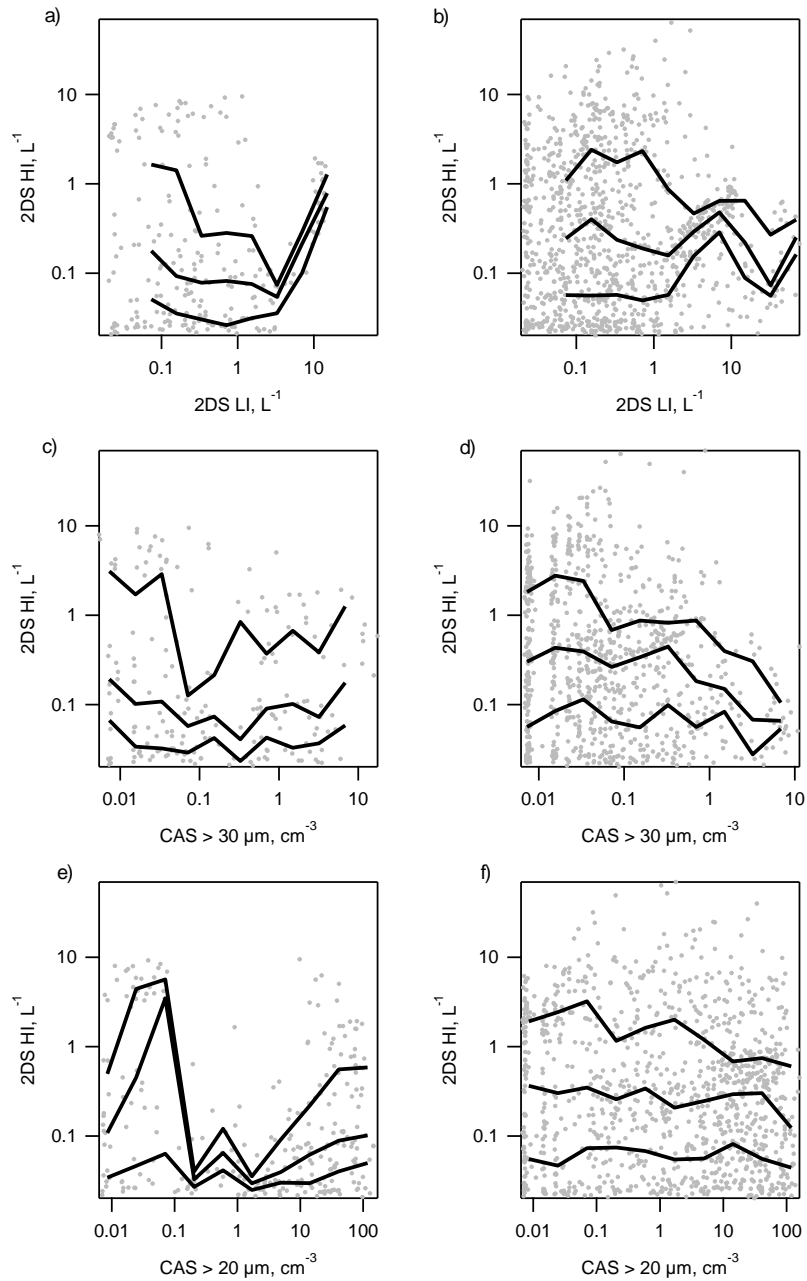
1
 2 *Figure 4. Box and whisker plots summarising in cloud measurements (averaged over 10 s) as*
 3 *a function of temperature. Plate a) shows the concentration of cloud droplets (cm^{-3}),*
 4 *measured by CAS, while b) shows the concentration of ice particles measured by 2DS and*
 5 *CIP-25, based on those classified as highly irregular (see text for details). The concentration*
 6 *of ice nucleating particles predicted by the DeMott et al. (2010) parameterisation with a high*
 7 *(1 scm^{-3}) and low (0.1 scm^{-3}) aerosol input are shown as dark and light blue lines, respectively*
 8 *in b). The green line is the predicted ice particle concentration according to the Cooper*

1 (1986) parameterisation. c) a histogram of the flight distance while continuously sampling
2 ice.

3

4 Previous observations of Arctic mixed phase clouds found that the presence of precipitating
5 ice particles ($> 400 \mu\text{m}$) was associated with the number of large drops ($>30 \mu\text{m}$), however
6 the precise nucleation mechanism through which this occurs is uncertain (Lance et al., 2011).
7 To identify if a similar relationship was present during MAC Fig. 5a,b shows the relationship
8 between the 2DS HI and the 2DS LI particles (droplets larger than approximately $80 \mu\text{m}$).
9 Figures 5c,d and 5e,f show similar plots for the CAS measurements of droplets larger than 30
10 and $20 \mu\text{m}$, respectively. Panels on the left (a, c and e) show measurements at temperatures
11 lower than -8°C and panels on the right (b, d and f) show those in the range -8 to 0°C . The HI
12 concentrations are binned based on the droplet concentration and the 25, 50 and 75 percentiles
13 are shown as black lines. When examining statistics for all stratus flights we find no evidence
14 that the ice concentrations increase due to the presence of large drops. However, any
15 relationship may be obscured as drops are depleted by ice crystal growth through riming and
16 the Wegener-Bergeron-Findeisen process.

17



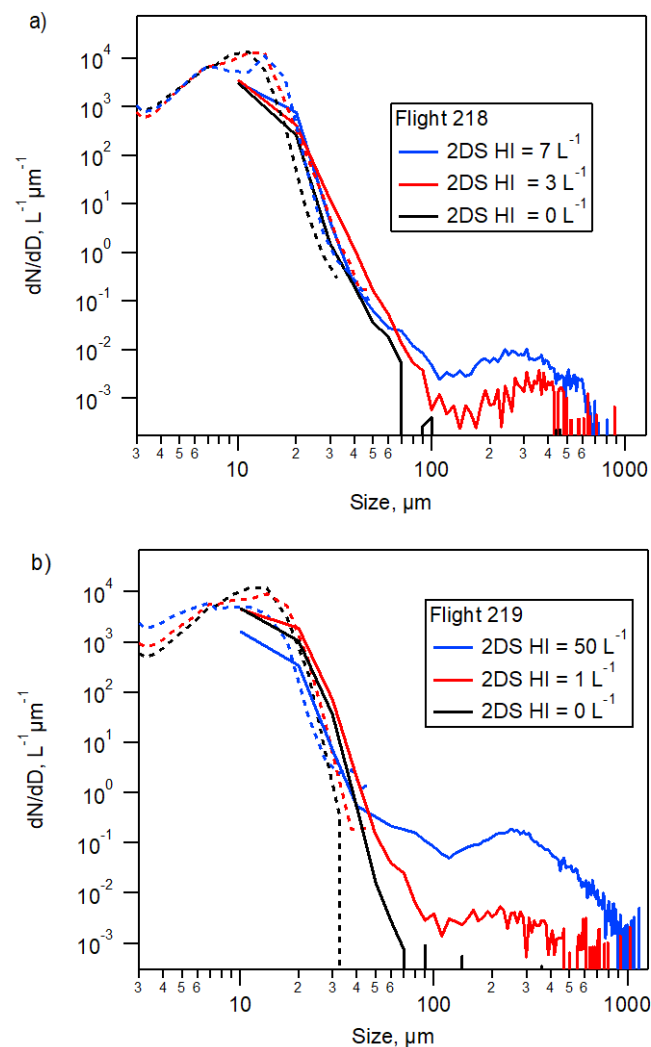
1

2 *Figure 5a,b. The relationship between the concentration of highly irregular (2DS HI)*
 3 *particles and low irregular particles (2DS LI) (low irregular particles greater than*
 4 *approximately 80 μm). Figures 6c,d and 6e,f show the relationship with the concentration of*
 5 *droplets larger than 30 and 20 μm, respectively. Panels on the left (a, c and e) show*
 6 *measurements at temperatures lower than -8°C and panels on the right (b, d and f) show*
 7 *those in the range -8 to 0 °C. The black lines are the 25th, 50th and 75th percentile of the 2DS*
 8 *HI concentration for each droplet concentration bin.*

9

1 Similar results are found when case studies for individual flights are examined. Figure 6a
 2 shows a comparison between the particle size distributions for three periods with quite
 3 different degrees of glaciation during a constant altitude run at $-5\text{ }^{\circ}\text{C}$ during Flight 218. Time
 4 series of the microphysical properties during this run are shown in Fig. 7. During this run
 5 there were patches of ice with concentrations of several per litre and regions where no ice was
 6 present. However, there are no distinct differences in the particle size distributions for
 7 particles $<100\text{ }\mu\text{m}$ for these three cases. Figure 6b shows a similar plot for a constant altitude
 8 run at $-6\text{ }^{\circ}\text{C}$ during Flight 219. During times with very high ice concentrations (2DS HI up to
 9 50 L^{-1} , blue line) the droplets (10s minimum of 11 cm^{-3}) are depleted compared to the cases
 10 when the 2DS HI concentration was 1 L^{-1} and 0 L^{-1} (approximately 100 cm^{-3}).

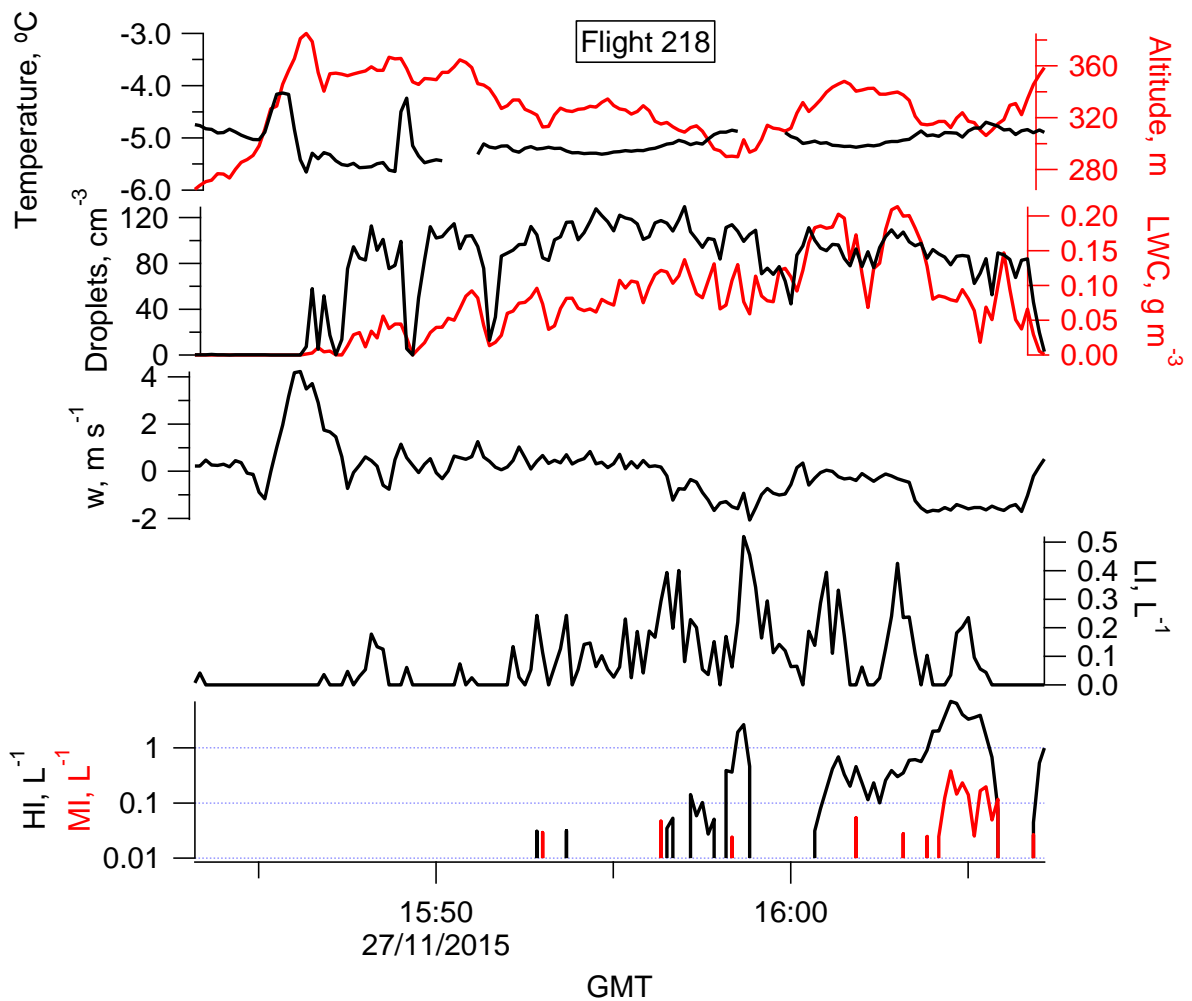
11



12

1 *Figure 6a. Comparison between the particle size distributions for 3 regions sampled in the*
 2 *constant altitude run at -5 °C during Flight 218, these are where the concentration of highly*
 3 *irregular particles (2DS HI) was 7 L⁻¹ (16:04 GMT), 3 L⁻¹ (15:58 GMT) and 0 L⁻¹ (15:52*
 4 *GMT). Time series of the microphysical measurements during this run are shown in Figure 8.*
 5 *Figure 7b shows a similar plot for a run at -6 °C during Flight 219 when the 2DS highly*
 6 *irregular concentration was 50 L⁻¹, 1 L⁻¹ and 0 L⁻¹. Dashed lines show measurements from the*
 7 *CAS and solid lines are from the 2DS.*

8



9

10 *Figure 7. Time series of microphysical parameters during a constant altitude run at -5°C*
 11 *(400 m) during flight 218.*

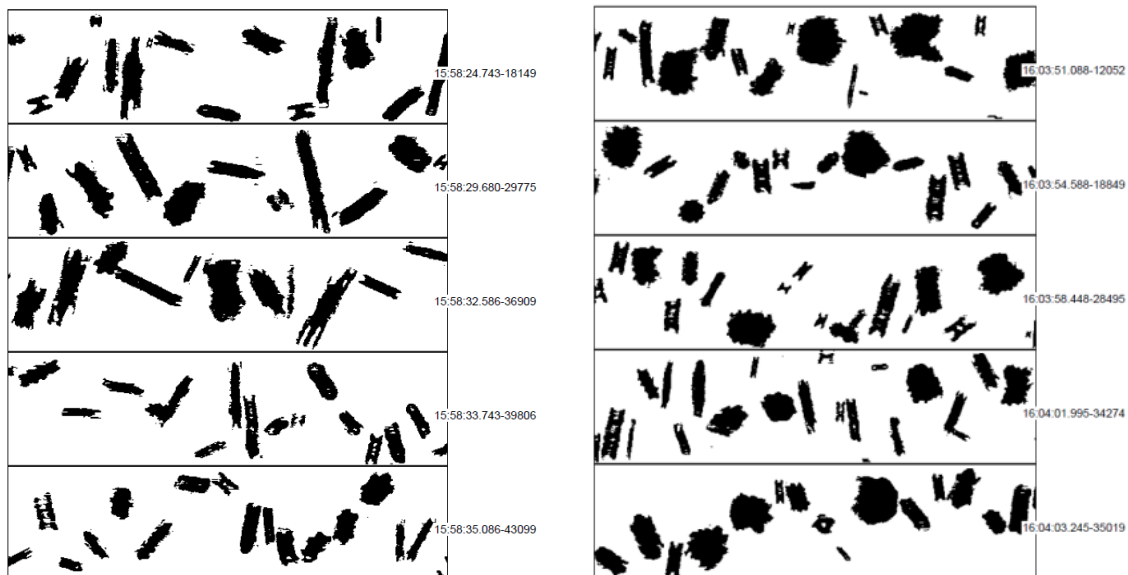
12

13

1 3.1.1 Ice Crystal Images

2 Inspection of the cloud particle images shows that at temperatures higher than $-10\text{ }^{\circ}\text{C}$
3 columnar crystals appear as the dominant ice crystal habit, with irregular rimed crystals also
4 widespread. This is illustrated by Fig. 8a showing example images from Flight 218 at $-5\text{ }^{\circ}\text{C}$.
5 Measurements in Arctic clouds at similar temperatures show that they are similarly dominated
6 by columnar crystals (Lloyd et al., 2015a). Figure 8b. shows images at $-15\text{ }^{\circ}\text{C}$ collected in a
7 single layer cloud over the Antarctic continent, approximately 300 km south of Halley (Flight
8 233). This cloud had some columns/needles, but also a high proportion of plates and stellar
9 crystals. At the lowest sampled temperatures of $-20\text{ }^{\circ}\text{C}$ (Fig. 8c, Flight 226) the ice mostly
10 consists of rosettes and irregular crystals, which may be aggregates. However, measurements
11 at these low temperatures were relatively infrequent, and the ice may have been nucleated at
12 lower temperatures higher in the cloud.

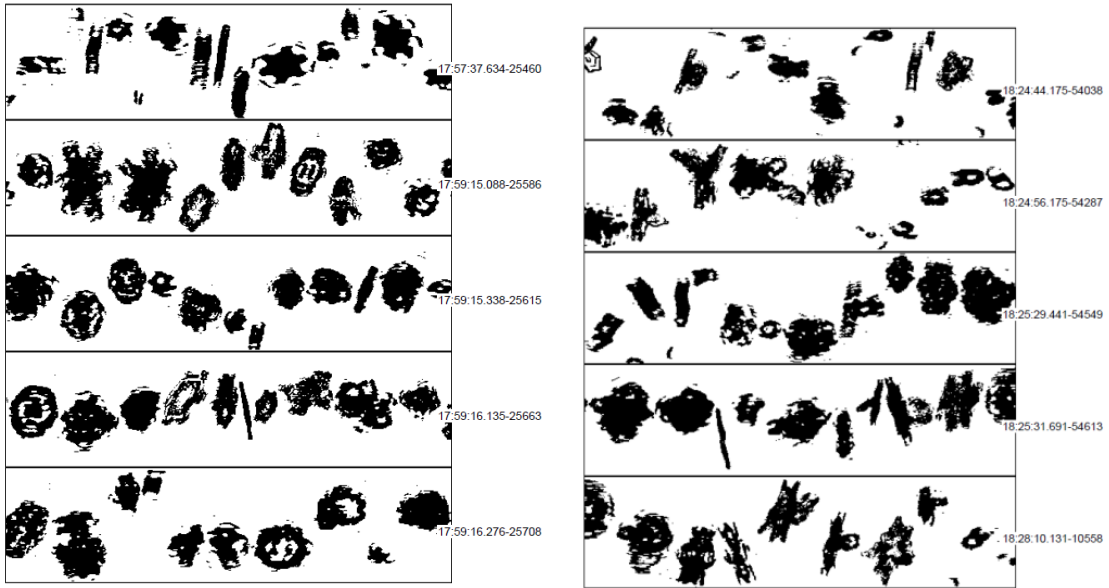
13



14

15 *Figure 8a. 2DS Images of highly irregular particles during a constant altitude run at $-5\text{ }^{\circ}\text{C}$*
16 *(400 m) during flight 218. The times given are for the first crystal on each strip. The height of*
17 *each strip corresponds to the 2DS array width of $1280\text{ }\mu\text{m}$.*

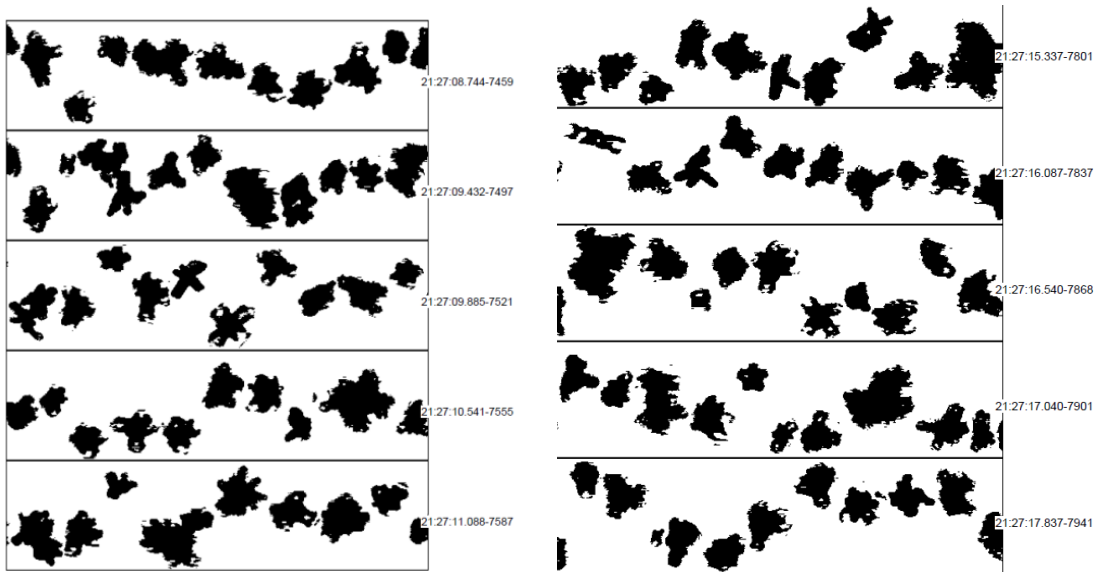
18



1

2 *Figure 8b. 2DS Images of highly irregular particles during a constant altitude run at -15°C*
 3 *during flight 233.*

4



5

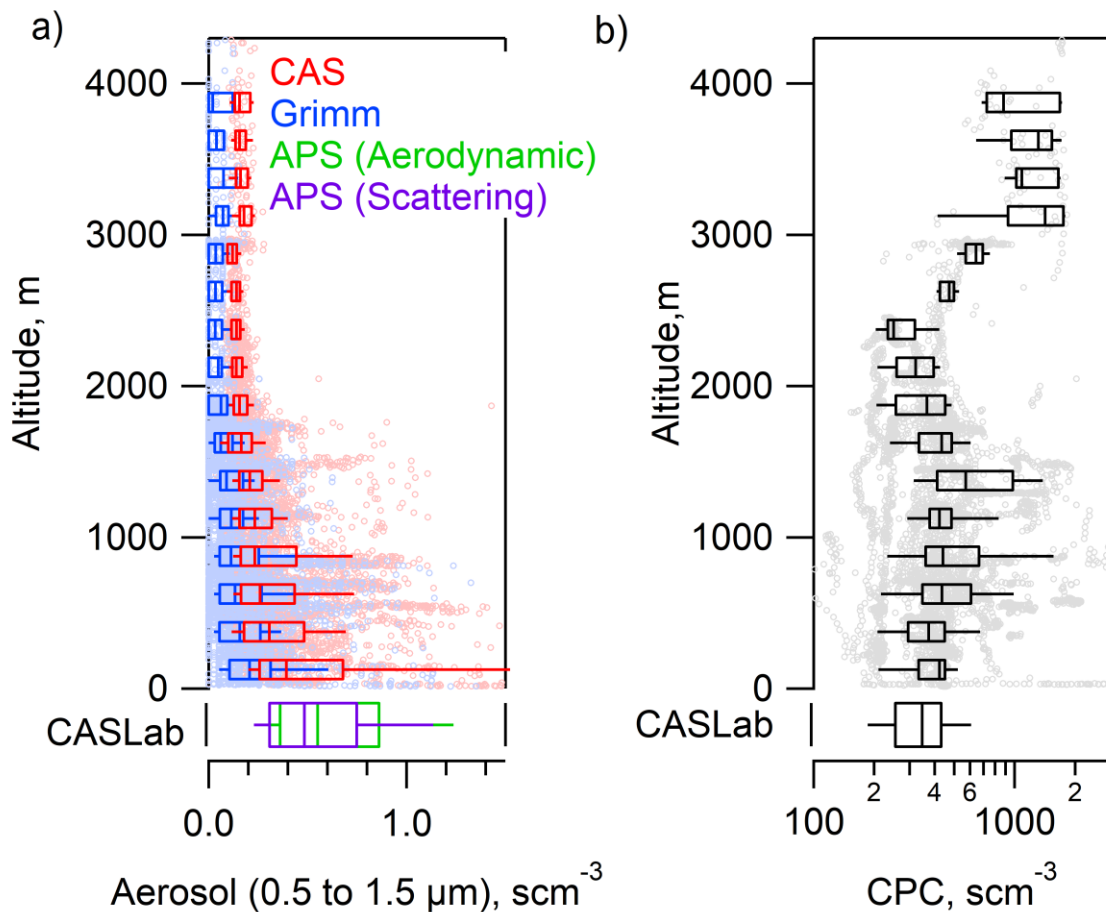
6 *Figure 8c. 2DS Images of highly irregular particles during a constant altitude run at -20°C*
 7 *during flight 226.*

8

1 3.2 Aerosol

2 Vertical profiles of the out-of-cloud aerosol measurements made by the aircraft are shown in
3 Fig. 9. Out-of-cloud measurements were selected as periods when the LWC was less than
4 0.001 g m^{-3} and when the 2DS was not detecting particles. Contributions from large, swollen
5 aerosol particles were also removed when the relative humidity was higher than 90%.
6 Figure 11a shows aerosol concentrations over the size range from 0.5 to $1.5 \text{ }\mu\text{m}$ as observed
7 by the CAS and GRIMM probes. This size range of aerosols has been shown to best represent
8 the concentration of INPs in many locations around the world (DeMott et al., 2010).
9 Concentrations within this size range decrease significantly with increasing height, as would
10 be expected, through sea spray aerosol being rapidly removed by cloud processing or
11 sedimentation. Previous, measurements over the Antarctic Peninsula also found that aerosols
12 in this size range decreased with height and ranged between 0.1 and 0.3 cm^{-3} above
13 approximately 2500m . Total aerosol concentrations, measured by the CPC during MAC, had
14 a median value for the campaign of 408 scm^{-3} (at standard temperature and pressure) and an
15 inter-quartile range of 260 scm^{-3} .

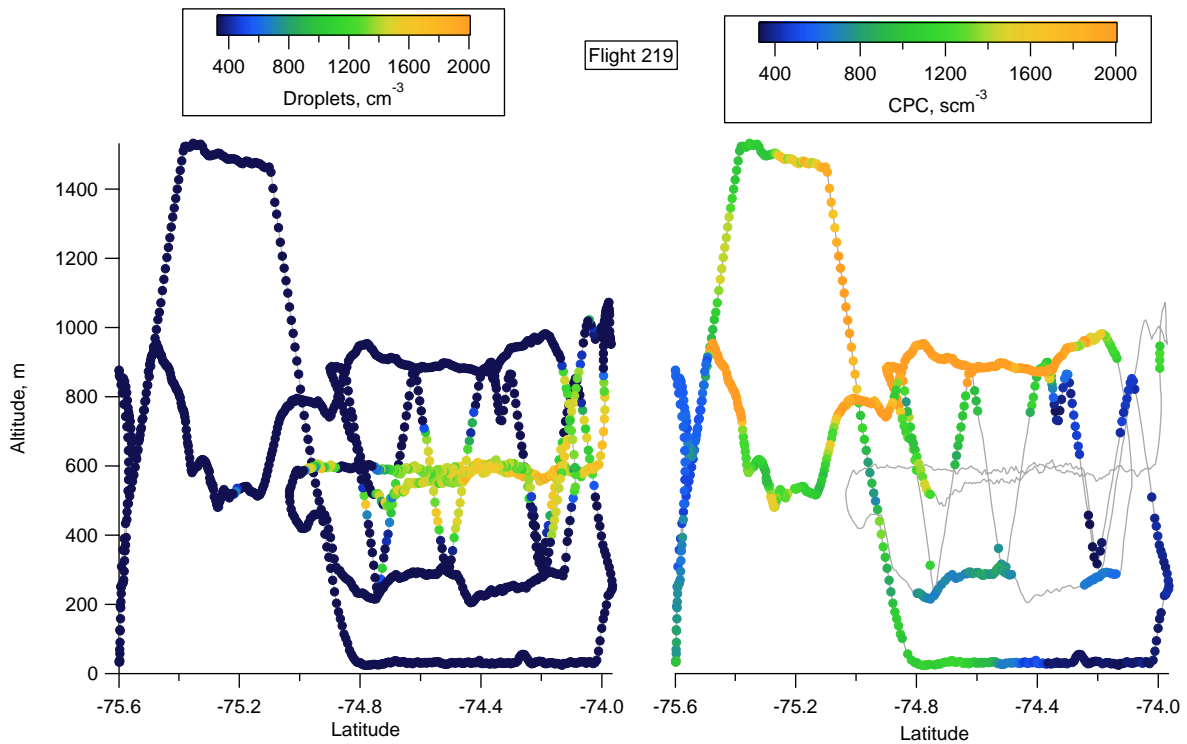
16



1
 2 *Figure 9. Aircraft clear sky aerosol concentrations (scm^{-3}) altitude profiles. Data are from: a)*
 3 *CAS and GRIMM instruments. Surface concentrations from CASLab are shown for*
 4 *comparison, from the APS; Green - aerodynamic particle size concentrations; Purple –*
 5 *scattering cross section derived particle size concentration measurements; b) Total fine*
 6 *aerosol concentration profiles, from CPCs on the aircraft and at the CASLab, ($D > 10 \text{ nm}$).*

7
 8 During MAC episodic periods were observed with total aerosol concentrations in excess of
 9 1000 scm^{-3} . These were often observed above cloud layers. The flights were designed to focus
 10 on cloud regions so may not represent a truly unbiased sample of the atmosphere, but the
 11 results do suggest a link between the observations of high aerosol concentrations and the
 12 presence of clouds. The limited spatial coverage of the aircraft measurements makes
 13 quantifying the extent of these layers uncertain, however they appear to extend over a few
 14 tens of kilometres to a hundred kilometres. At least two instances (flights 218, 219, see Fig.
 15 10) suggest a large layer extending beyond the cloud edge, pointing at the possibility of layers
 16 independent from clouds. The peak concentration usually occurred in the region up to 200 m

1 above the cloud top (e.g. Flight 219). Some layers showed a clear drop in relative humidity
 2 (e.g. from 90% to 30%, e.g. during flight 220, 221, and 222) generally related to a clear
 3 temperature inversion, while other layers showed a much smaller decrease (by 10%) in
 4 relative humidity compared to the cloud underneath (e.g. flight 217, 218, 219). No clear
 5 systematic relationship was observed with respect to the vertical wind velocity (turbulence).
 6 The role of these particles as CCN/INPs is currently uncertain due to the lack of information
 7 about their composition.



8
 9 *Figure 10. Latitudinal cross-sections of Flight 219 coloured by droplet concentration (left*
 10 *panel) and total aerosol concentrations out of cloud (right panel). Grey lines shows the flight*
 11 *track. These show a layer of high aerosol concentrations above the cloud top.*

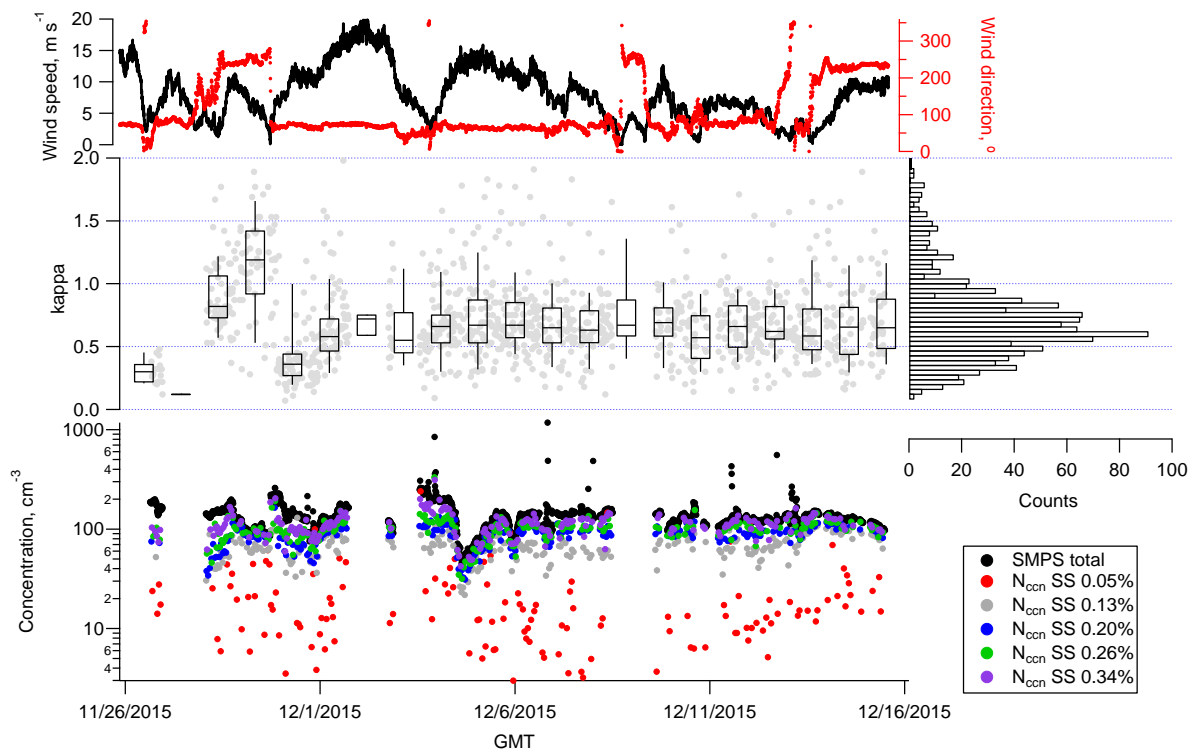
12
 13 Average total concentrations of UV-fluorescent aerosols (measured at CASLab with the
 14 WIBS) over the campaign period were $\sim 1 \text{ L}^{-1}$, which was $< 2\%$ of the total particle
 15 concentration. Of these 0.01 L^{-1} were identified as likely primary biological aerosols. During
 16 some Easterly and Westerly wind events, however, enhanced concentrations of the order of
 17 $5 \pm 7 \text{ L}^{-1}$ could be observed (Crawford et al., 2017).

18

1 3.3 Cloud condensation nuclei (CCN)

2 Figure 11 (bottom panel) summarises the CCN measurements at the CASLab. The bottom
3 panel shows the CCN at 5 different super saturations (0.05%, 0.13%, 0.20%, 0.26% and
4 0.34%). The hygroscopicity parameter κ is used to examine the effect chemical composition
5 has on the CCN activity of aerosol particles. The derived κ values represent the average
6 hygroscopicity of the volume-weighted fractions of the individual aerosol components. Non-
7 hygroscopic components have a κ value of 0. Highly CCN active salts have κ values between
8 0.5 and 1.4, sodium chloride (NaCl) has a κ of 1.28 (measurement range 0.91 to 1.33).
9 Organic species have values generally between 0.01 and 0.5 (Petters and Kreidenweis, 2007).
10 The median κ value during MAC was 0.64 (inter-quartile range = 0.34, mean = 0.69),
11 suggesting that this location is dominated by hygroscopic components, such as sea-salt and
12 sulphate. Andreae and Rosenfeld (2008) review CCN measurements and find that κ values
13 from marine locations generally cover a relatively narrow range of 0.7 ± 0.2 , compared to 0.3
14 ± 0.1 for continental aerosols. A global model study subsequently presented a mean κ value of
15 0.92 (0.09 at 1σ) at the surface and 0.80 (0.17 at 1σ) within the boundary layer over the
16 Southern Ocean (Pringle et al., 2010), only marginally higher than our MAC observations.

17



18

1 *Figure 11. The top panel shows the time series of wind speed (black line) and direction (red*
2 *markers) at the CASLab. The middle panel shows the time series of the hygroscopicity*
3 *parameter κ . The box and whisker plots summarise the variability in κ for each day, while the*
4 *right panel shows a histogram of κ for the whole measurement period. The bottom panel*
5 *shows the total aerosol number from the integrated SMPS measurements (30 to 500 nm, black*
6 *dots) and the CCN concentrations at 5 different supersaturations (SS, coloured dots from 0.05*
7 *to 0.34%).*

8

9 As shown in Fig. 11 there was a period of increased hygroscopicity on 28 and 29 November
10 2015, with a median κ of 1.18 on 29 November. During this period there was a westerly wind.
11 This changed to an easterly on 30 November 2015, which coincided with a decrease in
12 hygroscopicity to a median κ for the 30 November of 0.36. Between the approximate
13 headings 210° to 25° the CASLab lies between 30 and 60 km from the Weddell Sea. In
14 contrast, within the sector 30° to 60° it lies several hundred km across the Brunt Ice Shelf
15 from the Weddell Sea. To the south east of the CASLab lies the Antarctic Continent.
16 HYSPLIT trajectories indicate over the past 5 days the airmass sampled on 28 and 29
17 November 2015 had passed over sea ice/open water regions. However after 30 November
18 2015 the hygroscopicity was relatively consistent and does not show a significant relationship
19 with the wind direction or airmass history. For example, on the 14 and 15 December 2015
20 there was a westerly wind but the median κ for these days of 0.66 and 0.65, respectively, was
21 similar to the campaign median (0.64).

22 **3.4 Ice nucleating particles (INPs)**

23 Ice nucleating particles (INPs) could not be directly measured on the aircraft during MAC.
24 Instead we compare the cloud ice crystal concentrations with two parameterisations that are
25 commonly used to predict INP concentrations. DeMott et al. (2010) compiled INP
26 measurements from a range of locations around the world and derived a relationship using
27 aerosol concentrations (within the size range 0.5 to 1.6 μm) and temperature that could
28 explain the INP variability within their dataset to better than a factor of 10. For a broad
29 comparison with the MAC dataset we evaluate DeMott et al. (2010) for a high (1 scm^{-3} , dark
30 blue lines, Fig. 4b) and low (0.1 scm^{-3} , light blue lines, Fig. 4b) aerosol case. Cooper (1986)
31 describes a simple INP parameterisation using only the ambient temperature, which is often

1 used in the Weather Research Forecasting model (WRF) (Morrison et al., 2009). The
2 concentration of INPs from Cooper (1986) is shown as a red line in Fig. 4b. It should be noted
3 that neither of these parameterisations use Antarctic measurements. Given the marine location
4 of the flights it is likely that these parameterisations may represent overestimates of the true
5 INP concentration, since the number of INP in sea spray aerosol is generally several orders of
6 magnitude lower than the number of INP in aerosol in the continental boundary layer (DeMott
7 et al., 2015). The DeMott et al. (2010) parameterisation was derived using measurements at
8 temperatures lower than -9°C , while Cooper (1986) used measurements below -5°C . For
9 comparison they are extrapolated to higher temperatures and are therefore subject to increased
10 uncertainty.

11 As shown in Fig. 4b, given the uncertainty in both parameterisations and the challenges with
12 making a direct comparison with the measurements it is plausible that the observed ice
13 concentrations at temperatures lower than about -10°C could be explained by primary ice
14 production. However above this temperature the measured ice concentrations diverge from
15 the predicted INP by 1 to 3 orders of magnitude, suggesting that secondary ice production is
16 becoming increasingly dominant.

17 Below -9°C , where secondary ice production is likely to be less significant, Listowski and
18 Lachlan-Cope (2017) found that the number of INP predicted by DeMott et al. (2010) gave
19 better agreement with observed ice concentrations over the Antarctic Peninsula compared to
20 INP parameterisations that only use the ambient temperature as input. For MAC, each in
21 cloud data point was compared with the closest (in time) out-of-cloud aerosol measurement (1
22 minute average, $\text{RH} < 90\%$). Data points were excluded from the comparison if no out-of-
23 cloud aerosol measurements were made within 10 minutes of the in-cloud measurement. No
24 clear relationship was found between the local aerosol concentrations and the ice
25 concentrations ($R^2=0.02$ for the above cloud aerosol in the size range 0.5 to $1.6\ \mu\text{m}$). During
26 MAC, the majority of cloud measurements showed no ice (see Fig. 3) suggesting that the
27 Antarctic is a very low INP environment. As a result, all conventional INP schemes will
28 likely overestimate the true concentrations.

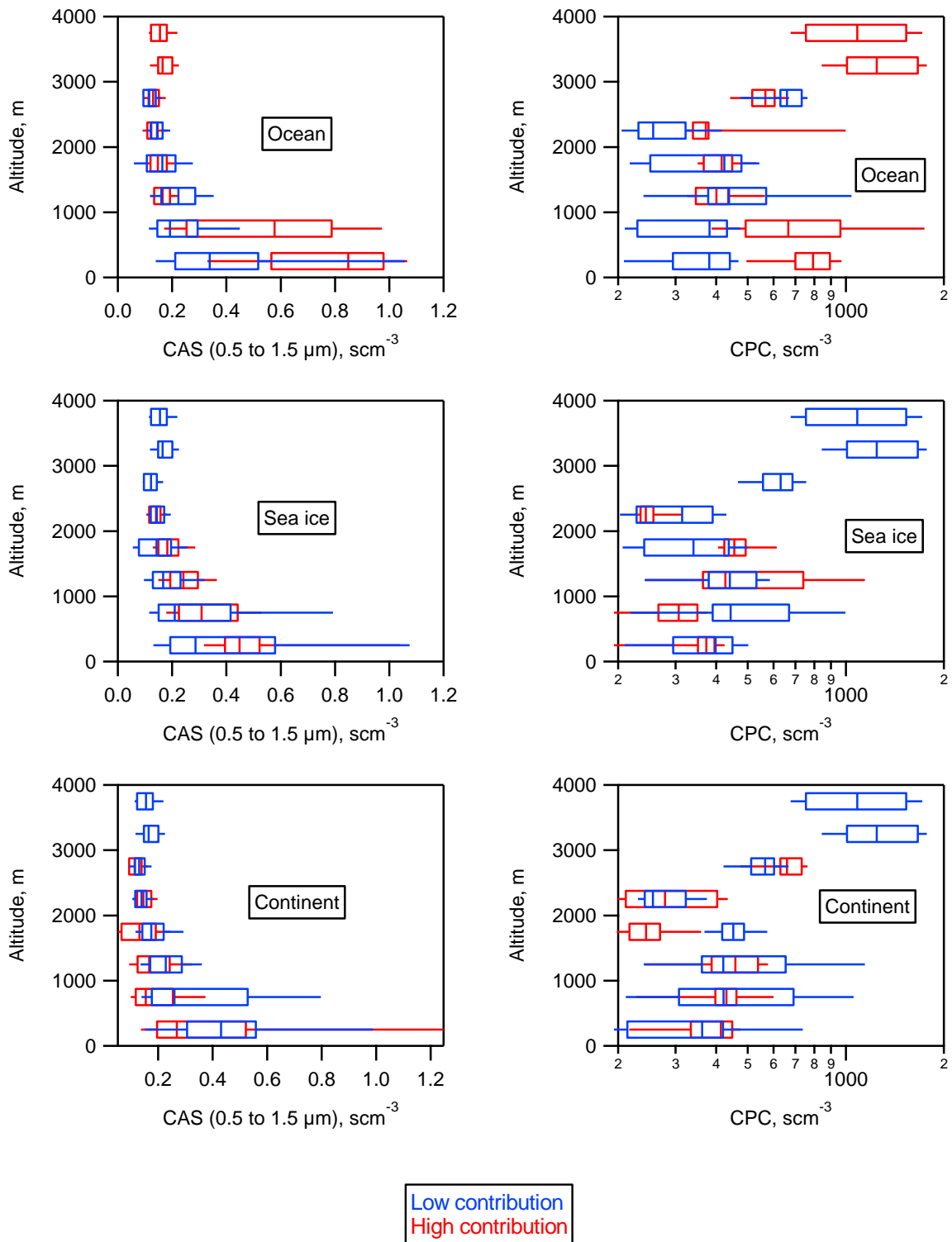
29

1 **3.5 Airmass history**

2 The sampled airmasses were classified based on their time spent over different geographic
3 regions (see Sect. 2.4). Figure 12 shows vertical profiles of the aerosol from the CAS (0.5 to
4 1.5 μm , relative humidity < 90%) when there was high (>50%, red markers) and low (<50%,
5 blue markers) surface influence from the Southern Ocean, the sea ice and the Antarctic
6 Continent. There is a broad trend of higher aerosol concentrations over this size range with
7 greater contributions from the Ocean and sea ice, indicating significant emissions of sea
8 salt/sulphate aerosol. Concentrations decrease with increased contributions from the
9 continent, indicating a lack of sources in this region. These relationships are more distinct
10 when the aircraft was sampling at low altitude, above approximately 1000 m the
11 concentrations are less dependent on airmass origin due to their lower surface influence. This
12 analysis was repeated using total aerosol concentrations from the CPC (Fig. 14). Similar to
13 the CAS, higher concentrations were observed when there was greater influence from the
14 Southern Ocean, with the differences again most distinct for the low altitude measurements.
15 However, CPC concentrations are found to be less dependent on the influence of the sea ice
16 and the Antarctic Continent.

17

18



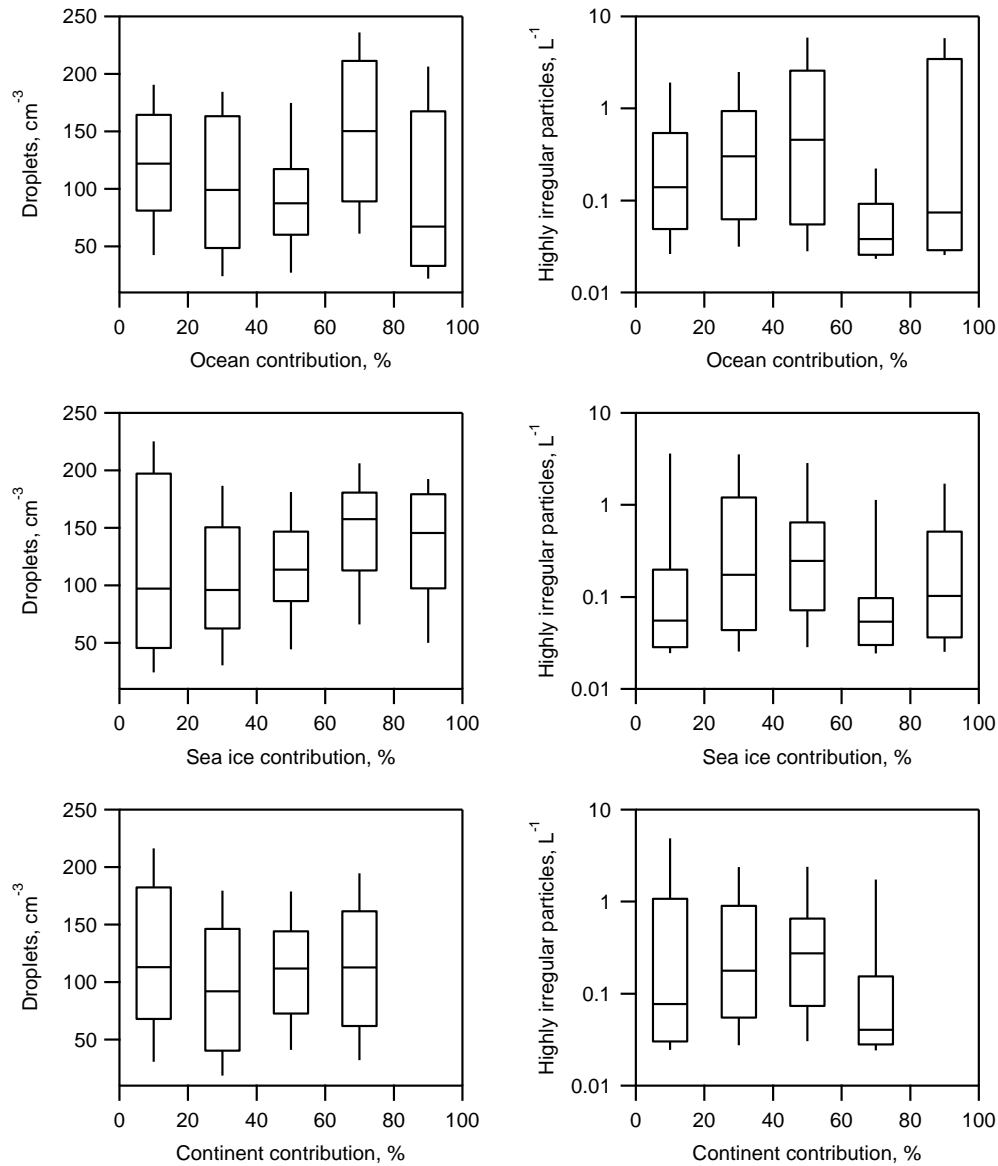
1

2 *Figure 12. Altitude profiles of CAS aerosol over the size range 0.5 to 1.5 μm (left panels) and*
 3 *total aerosol, greater than 10nm from the CPC (right panels). The measurements have been*
 4 *partitioned into periods when the airmass had a high (red) and low (blue) contributions from*
 5 *different geographic regions (see text for details).*

1

2 Compared to the aerosol measurements the concentrations of cloud droplets and 2DS irregular
3 particles are found to be less dependent on air mass history. Figure 13 shows these variables as
4 a function of the relative surface influence from the Southern Ocean, sea ice and the
5 continent. The concentration of ice in the clouds is found to decrease for air masses with
6 increasing influence from the ocean. However, due to ice in the clouds being relatively
7 infrequently observed the significance of this relationship cannot be determined. The effects
8 of air mass history cannot easily be deconvolved from differences in sampling strategy or
9 cloud properties (e.g. humidity, temperature, dynamics, and secondary ice production). The
10 strongest relationship between aerosols and air mass history is for particles 0.5 to 1.5 μm this
11 is only a small proportion of the total CCN. While the CPC will observe the CCN but also
12 smaller particles. Also, given that the majority of measurements were conducted over broken
13 sea ice, it may be that the CCN origin may be more local and not show up in the far field
14 trajectories.

15



1

2 *Figure 13. The concentration of cloud droplets and 2DS highly irregular particles as function*
 3 *of the airmass's contribution from the Southern Ocean, sea ice and the continent (see text for*
 4 *details). Boxes give the 25th and 75th and the whiskers are the 10th and 90th percentiles for*
 5 *each regional contribution bin.*

6

7 **4 Discussion**

8 This section summarise the observations presented in the paper and discusses the important
 9 microphysical processes. The cloud types were generally stratus, both single and multiple
 10 layers, predominantly between -20 and -3 °C. These were dominated by super cooled liquid
 11 drops, with a median concentration of 113 cm^{-3} . Droplet concentrations were relatively

1 consistent during the campaign with an inter-quartile range of 86 cm^{-3} . The exceptions to this
2 were when the droplets were depleted by high ice concentrations and also flight 217 where
3 anomalously high droplet concentrations were observed, which was associated with an
4 enhanced aerosol layer below cloud. Similar to Arctic layer clouds (McFarquhar et al., 2007),
5 liquid content and cloud drop effective radius both increased with distance from cloud base
6 likely due to condensational growth. Collision coalescence may also have contributed to this
7 increase in effective radius. However, droplet number concentration was relatively invariant
8 to position within the cloud.

9 Ice in the clouds exhibited a high degree of variability, occurring in small patches. Constant
10 altitude runs by the aircraft through clouds at slightly supercooled temperatures ($> -10^\circ\text{C}$)
11 showed ice-free regions with patches of high ice concentrations ($>1 \text{ L}^{-1}$). This variability is
12 shown to exist over small spatial scales and may be a consequence of very low INP
13 concentrations, where secondary processes may significantly amplify small differences in INP
14 concentrations. This makes predicting in detail where ice will form in a given cloud extremely
15 challenging. A detailed understanding of where the first ice will occur and also the conditions
16 required for secondary production is needed. Here we examine this variability and discuss
17 some of the potential controlling factors.

18

19 **4.1 First Ice**

20 First we examine the nature and sources of the INP. Global primary ice nucleation below
21 approximately -15°C is thought to be dominated by soot and mineral dusts (Möhler et al.,
22 2006; Murray et al., 2012; Niemand et al., 2012). However, this is colder than the cloud top
23 temperatures generally observed during MAC. Biological species (pollen, bacteria, fungal
24 spores and plankton) are the only INP that are known to be active at temperatures higher than
25 approximately -15°C (Alpert et al., 2011; Murray et al., 2012; Wilson et al., 2015). Bioaerosol
26 measurements at the CASLab show episodic high concentrations up to several per litre. This
27 temporal variability in bioaerosol may be analogous to the spatial variability of the ice
28 crystals observed in the clouds. Source apportionment of the bioaerosol at Halley is uncertain
29 with the available dataset, but may include contributions from 1) the re-suspension of material
30 from the local ice and snow surface, 2) coastal ice margin zones in Halley Bay where bird

1 colonies are present and 3) long-range transport. The bioaerosol measurements will be
2 presented and discussed in detail in a separate paper.

3 It is possible that the cloud layers sampled in MAC are seeded by precipitation from higher
4 layers where the temperatures are low enough for dust to be active as an INP. During MAC
5 the flights were designed so that measurements were performed between cloud layers to
6 determine whether ice seeding from the upper layers was occurring. The frontal cloud
7 sampled in flight 224 showed extensive ice precipitating between cloud layers and the cloud
8 top temperature (below $-20\text{ }^{\circ}\text{C}$) was sufficiently low for dust to be a potential source of ice
9 nuclei. In the case of stratus clouds, those were not found to be seeded by layers at low
10 enough temperatures for any dust to be active as an INP. Furthermore, single layer clouds
11 such as those sampled in flights 219 and 227 still showed the patchy ice behaviour.

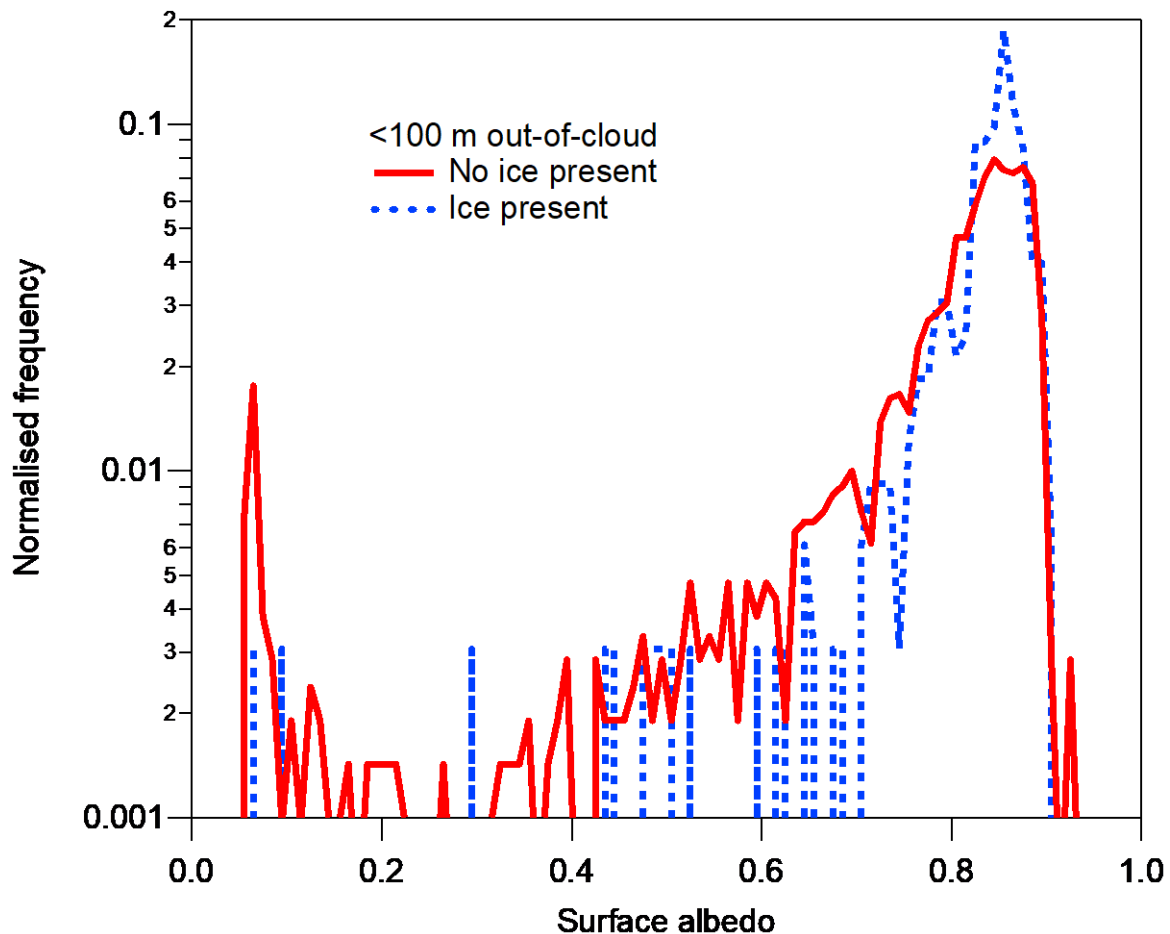
12 Detailed measurements of aerosol composition were not available on the aircraft. No clear
13 relationship could be identified between the local aerosol concentrations (both above and
14 below cloud) and the presence of ice in the clouds. However, only a small proportion of the
15 total aerosol population are expected to be INP. Below approximately 2000 m (where most of
16 MAC measurements were performed) there is a broad trend of ice being more frequent with
17 decreasing altitude. A similar relationship is observed for the concentration of particles
18 between 0.5 and $1.6\text{ }\mu\text{m}$ (Fig. 9). However, this may in part be due to secondary ice
19 production being efficient at these relatively high temperatures. Jackson et al. (2012) found a
20 correlation ($R=0.69$) between the above cloud aerosol ($0.1 < D < 3\text{ }\mu\text{m}$) and ice
21 concentrations in Arctic stratocumulus clouds. However these clouds were generally at lower
22 temperatures (cloud top temperature $< -10^{\circ}\text{C}$) than those during MAC and as a result are
23 likely to have a higher proportion of primary ice production.

24 The surface may also be an ice crystal source either through blowing snow (Ardon-Dryer et
25 al., 2011) or frost flowers (Gallet et al., 2014; Lloyd et al., 2015b). These will be most
26 important for clouds in contact with the surface (Vali et al., 2012), but may also be relevant
27 for low clouds when the humidity is sufficiently high that the crystals do not evaporate whilst
28 being transported to the cloud base (Geerts et al., 2015). Space-borne lidar measurements of
29 blowing snow over Antarctica found the thickness of these layers ranging between their
30 detection limit (30 m) up to 1000 m, with an average thickness of 100 m. Approximately 71%
31 of these layers were less than 100 m thick and 25% were between 100 and 300 m thick (Palm
32 et al., 2011). Similarly, lidar measurements at the South Pole found that layers were generally

1 less than 400 m thick (63%), but could be up to 1000 m thick. Blowing snow is almost always
2 constrained to the planetary boundary layer (Mahesh, 2003). The lofting of snow is complex;
3 it is dependent on a range of variables, including: the snow type and surface meteorology (e.g.
4 wind speed, turbulent mixing, temperature and humidity). A threshold wind speed of 7 to 10
5 m s^{-1} is typically required (Dery and Yau, 1999). However, smaller crystals may show
6 substantial fluxes at lower wind speeds. Aerosol fluxes from evaporated frost flowers have
7 been estimated at $10^{-6} \text{ m}^{-2} \text{ s}^{-1}$ at wind speeds as low as 1 m s^{-1} (Xu et al., 2013).

8 Evaluating the impact of these mechanisms during MAC is challenging since most of the in-
9 cloud sampling was performed over snow covered sea ice, making it difficult to attribute local
10 differences in the microphysics to the surface type. Figure 14 shows histograms of the surface
11 albedo for out-of-cloud measurements (below 100 m) when there was (blue line) and was not
12 (red line) ice observed. Here the surface albedo is used as a proxy for the surface type, since
13 values near 0 correspond to overflying open water and the values near 1 correspond to a
14 snow/ice covered surface. Figure 14 suggests that ice measured by the aircraft while out cloud
15 (below 100 m) almost exclusively occurred when overflying a snow/ice covered surface,
16 implying a link between the surface type and the presence of ice in the clouds. The ice
17 measured on the aircraft when out-of-cloud could either have originated from the surface or
18 precipitated from clouds above. However, it should be noted that very few measurements
19 were made over open water regions.

20



1
 2 *Figure 14. Histograms of the surface albedo for of out-of-cloud measurements (below 100 m)*
 3 *when there was (blue line) and was not (red line) ice detected.*

4
 5 Flight 218 (Fig. 7) is one case where the first ice development may be due to surface ice
 6 crystals. During this flight ice was observed precipitating below cloud base. The majority of
 7 this ice precipitation was detected when flying over snow covered sea ice rather than open
 8 water. Given the relatively low cloud base (300m), strong surface horizontal winds (5 to 10 m
 9 s^{-1}) and a relative humidity approaching 100% it is plausible that ice from the surface (e.g.
 10 from blowing snow) could mix up to cloud base, thus providing the first ice to the cloud. The
 11 sublimation rate of an ice crystal is largely dependent on the humidity. A 100 μm ice crystal
 12 at 0°C will have a lifetime of the order 100s at a relative humidity of 80%. At relative
 13 humidities of 90% and 95% the lifetime can be over 200 s and 400 s, respectively (Thorpe and
 14 Mason, 1966). The ice crystals below cloud had similar habits to those observed in the cloud
 15 (a mixture of columns and rimed crystals) indicating they had not originated from the surface.

1 However, only low concentrations of primary ice from the surface is needed if the ice is then
2 able to multiply within the cloud due to secondary processes (Crawford et al., 2012).

3

4 **4.2 Secondary Ice**

5 Previous ice crystal observations over the Antarctic Peninsula show a similar behaviour to
6 those during MAC with a peak in ice concentrations ($> 1 \text{ L}^{-1}$) at approximately -5°C .
7 Grosvenor et al. (2012) and Lachlan-Cope et al. (2016) attribute this to secondary ice
8 production through the Hallett-Mossop process, where ice splinters are produced when a
9 droplet freezes subsequent to colliding with an ice crystal (riming) (Hallett and Mossop,
10 1974). This can lead to rapid ice multiplication as the splinters freeze further drops, resulting
11 in more splinters. Laboratory experiments suggest that this process is efficient over a narrow
12 temperature range (-8 to -3°C) with a peak at -5°C (Mossop, 1976). Images from the 2DS
13 probe at temperatures higher than -10°C generally show rimed crystals and small columns
14 (Fig. 10a). These habits are generally observed when the Hallett-Mossop production
15 mechanism is thought to be occurring (Crosier et al., 2011; Lloyd et al., 2015a).

16 A number of other secondary ice mechanisms have previously been identified, these include:
17 large drops producing ice splinters when they freeze (Rangno and Hobbs, 2001; Lawson et
18 al., 2015); and the break-up of ice crystals, generally either fragile dendrites due to
19 sublimation, turbulence (Bacon et al., 1998) or because of collisions between crystals (Yano
20 and Phillips, 2011). However, all these processes have generally only been observed to be
21 efficient at temperatures lower than approximately -10°C , which is lower than the
22 temperature of the majority of clouds sampled during MAC. Taylor et al. (2015) suggest that
23 the drop-freezing secondary ice production, identified by Lawson et al. (2015), may have
24 occurred at temperatures higher than -10°C in their measurements of cumulus clouds.
25 However, they were not able to deconvolve its effects from the Hallett-Mossop mechanism.
26 We have not performed automatic habit recognition on the 2DS images taken during MAC,
27 however, inspecting the images “by-eye” suggests that the drop shattering events observed by
28 Lawson et al. (2015) were not common during MAC.

29 The exact requirements for secondary ice production through Hallett-Mossop are still
30 uncertain. It is thought that only a small amount of primary ice is needed for it to be
31 initiated, and recent model studies suggest this could be as low as 0.01 L^{-1} (Crawford et al.,

1 2012; Huang et al., 2017). Laboratory experiments suggest that production rates are
2 proportional to the accumulation of large drops ($>24 \mu\text{m}$) (Mossop and Hallett, 1974).
3 However, more recent field measurements found that estimated crystal production rates gave
4 better agreement with observed ice concentrations if this constraint on drop diameter was
5 removed (Crosier et al., 2011). Observations of Arctic mixed phase clouds found that the
6 presence of precipitating ice particles ($> 400 \mu\text{m}$) was correlated with the number of large
7 drops ($>30 \mu\text{m}$), however the precise nucleation mechanism through which this occurred was
8 uncertain (Lance et al., 2011). During MAC both the analysis of individual case studies and
9 the statistics for the whole campaign do not suggest that the concentration of large drops and
10 ice crystals were related. However, any simple relationship is likely to be complicated as ice
11 crystal growth will deplete the drops through riming and the Wegener-Bergeron-Findeisen
12 process. This is shown in Fig. 5 and 6b where the highest ice concentrations correspond to
13 relatively low droplet concentrations.

14 Flights 226, 227 and 228 involved sequential vertical profiles to examine the dependency of
15 ice on the clouds vertical structure. No link was identified between the presence of ice in the
16 vertical profile and local variations in cloud top temperature. However, since the first ice
17 occurs over small spatial scales, any relationship may be obscured by the aircraft's horizontal
18 motion whilst changing altitude. As a result the precise cloud top temperature, and its
19 variability, directly above the glaciated regions of the clouds is not known.

20

21 **5 Conclusions**

22 Understanding the cloud in the Antarctic is essential to accurate predictions of future climate
23 change. We have reported unique observations of cloud and aerosol properties over coastal
24 Antarctica and the Weddell Sea. The aerosol was predominantly hygroscopic in nature, with κ
25 being consistent with previous measurements and model predictions for remote locations
26 dominated by marine emissions. The concentration of large aerosols (0.5 to $1.6 \mu\text{m}$) decreased
27 with altitude, as would be expected, through sea salt/sulphate aerosol being rapidly removed
28 by cloud processing or sedimentation. Higher aerosol concentrations were observed in
29 airmasses that travelled over the Southern Ocean/sea ice compared to those from the main
30 Antarctic Continent.

31 In contrast to the aerosol concentrations, the droplet and ice concentrations showed minimal
32 dependence on airmass origin, it may be that the CCN origin may be more local and not show

1 up in the far field trajectories The cloud types were generally stratus, both single and multiple
2 layers, at temperatures between -20 and -3 °C. These were dominated by super-cooled liquid
3 drops, with a median concentration of 113 cm⁻³. Droplet concentrations were relatively
4 consistent throughout the campaign with an inter-quartile range of 86 cm⁻³. The exceptions to
5 this were cases when the concentrations became depleted by high ice concentrations, and also
6 during Flight 217 when anomalously high droplet concentrations were observed; this was
7 associated with an enhanced aerosol layer below the cloud layer. Both liquid water content
8 and drop effective radius increased near cloud top.

9 Ice in the clouds exhibited a high degree of inhomogeneity occurring in small patches. Below
10 approximately 2000 m ice was more frequent at higher temperatures, however even within the
11 -8 to -3 °C temperature range where Hallett-Mossop secondary production is most active, the
12 clouds were predominantly liquid. When ice was present within the temperature range -8 to -3
13 °C it seems likely that secondary ice production, through the Hallett-Mossop process, resulted
14 in concentrations that were 1 to 3 orders of magnitude higher than the number of INP
15 predicted by conventional primary ice nucleation schemes. The source of first ice in the
16 clouds is currently uncertain. First ice in the clouds often occurs at temperatures above -10
17 °C, this may be due to the presence of biogenic particles that are active INP at these
18 temperatures or alternatively (or indeed simultaneously) ice from the surface (e.g. blowing
19 snow or frost flowers) could be lofted into the clouds.

20 This paper has presented the most detailed in situ observations of coastal Antarctic clouds and
21 their surrounding aerosol properties to date. Upcoming studies will use the MAC observations
22 to test and improve the representation of Antarctic clouds in numerical weather/climate
23 models in this particularly important region.

24

25 **Acknowledgements**

26 The authors would like to thank Vicky Auld, Neil Brough and all the BAS staff who helped in
27 the Antarctic. We are grateful to Gillian Young for her assistance with the ERA interim
28 reanalysis data. The MAC project was funded by the UK Natural Environment Research
29 Council (Grant number: NE/K01482X/1).

30

1 **References**

- 2 Alpert, P. A., Aller, J. Y. and Knopf, D. A.: Initiation of the ice phase by marine biogenic
3 surfaces in supersaturated gas and supercooled aqueous phases, *Phys. Chem. Chem. Phys.*,
4 13(44), 19882, doi:10.1039/c1cp21844a, 2011.
- 5 Amato, P., Joly, M., Schaupp, C., Attard, E., Möhler, O., Morris, C. E., Brunet, Y. and Delort,
6 A. M.: Survival and ice nucleation activity of bacteria as aerosols in a cloud simulation
7 chamber, *Atmos. Chem. Phys.*, 15(11), 6455–6465, doi:10.5194/acp-15-6455-2015, 2015.
- 8 Andreae, M. O. and Rosenfeld, D.: Aerosol-cloud-precipitation interactions. Part 1. The
9 nature and sources of cloud-active aerosols, *Earth-Science Rev.*, 89(1–2), 13–41,
10 doi:10.1016/j.earscirev.2008.03.001, 2008.
- 11 Ardon-Dryer, K., Levin, Z. and Lawson, R. P.: Characteristics of immersion freezing nuclei at
12 the South Pole station in Antarctica, , (2008), 4015–4024, doi:10.5194/acp-11-4015-2011,
13 2011.
- 14 Asmi, E., Frey, A., Virkkula, A., Ehn, M., Manninen, H. E., Timonen, H., Tolonen-Kivimäki,
15 O., Aurela, M., Hillamo, R., and Kulmala, M.: Hygroscopicity and chemical composition of
16 Antarctic sub-micrometre aerosol particles and observations of new particle formation,
17 *Atmos. Chem. Phys.*, 10, 4253–4271, doi:10.5194/acp-10-4253-2010, 2010.
- 18 Bacon, N. J., Swanson, B. D., Baker, M. B. and Davis, E. J.: Breakup of levitated frost
19 particles, *J. Geophys. Res.*, 103(D12), 13763–13775, doi:10.1029/98JD01162, 1998.
- 20 Baumgardner, D., Jonsson, H., Dawson, W., O'Connor, D. and Newton, R.: The cloud,
21 aerosol and precipitation spectrometer: a new instrument for cloud investigations, *Atmos.*
22 *Res.*, 59–60, 251–264, doi:10.1016/S0169-8095(01)00119-3, 2001.
- 23 Baumgardner, D., Newton, R., Krämer, M., Meyer, J., Beyer, A., Wendisch, M. and
24 Vochezer, P.: The cloud particle spectrometer with polarization detection (CPSPD): A next
25 generation open-path cloud probe for distinguishing liquid cloud droplets from ice crystals,
26 *Atmos. Res.*, 142, 2–14, doi:10.1016/j.atmosres.2013.12.010, 2014.
- 27 Bigg, E. K.: Long-term trends in ice nucleus concentrations, *Atmos. Res.*, 25(5), 409–415,
28 doi:10.1016/0169-8095(90)90025-8, 1990.
- 29 Bodas-Salcedo, A., Williams, K. D., Field, P. R. and Lock, A. P.: The surface downwelling
30 solar radiation surplus over the southern ocean in the met office model: The role of

1 midlatitude cyclone clouds, *J. Clim.*, 25(21), 7467–7486, doi:10.1175/JCLI-D-11-00702.1,
2 2012.

3 Bodas-Salcedo, A., Hill, P. G., Furtado, K., Karmalkar, A., Williams, K. D., Field, P. R.,
4 Manners, J. C., Hyder, P., and Kato, S.: Large contribution of supercooled liquid clouds to the
5 solar radiation budget of the Southern Ocean, *J. Climate*, 29, 4213–4228, 2016.

6 van den Broeke, M. R., Bamber, J., Lenaerts, J. and Rignot, E.: Ice Sheets and Sea Level:
7 Thinking Outside the Box, *Surv. Geophys.*, 32(4–5), 495–505, doi:10.1007/s10712-011-9137-
8 z, 2011.

9 Bromwich, D. H., Nicolas, J. P., Hines, K. M., Kay, J. E., Key, E. L., Lazzara, M. A., Lubin,
10 D., McFarquhar, G. M., Gorodetskaya, I. V, Grosvenor, D. P., Lachlan-Cope, T. and Van
11 Lipzig, N. P. M.: Tropospheric clouds in Antarctica, *Rev. Geophys.*, 50(1), 1–40,
12 doi:10.1029/2011RG000363, 2012.

13 Bromwich, D. H., Otieno, F. O., Hines, K. M., Manning, K. W. and Shilo, E.: Comprehensive
14 evaluation of polar weather research and forecasting model performance in the antarctic, *J.*
15 *Geophys. Res. Atmos.*, 118(2), 274–292, doi:10.1029/2012JD018139, 2013.

16 Brown, P. and Francis, P.: Improved measurements of the ice water content in cirrus using a
17 total-water probe, *J. Atmos. Ocean.*, 1995.

18 Christner, B. C., Morris, C. E., Foreman, C. M., Cai, R. and Sands, D. C.: Ubiquity of
19 biological ice nucleators in snowfall., *Science*, 319(5867), 1214,
20 doi:10.1126/science.1149757, 2008.

21 Cooper, W. A.: Ice Initiation in Natural Clouds, *Meteorol. Monogr.*, 21(43), 29–32,
22 doi:10.1175/0065-9401-21.43.29, 1986.

23 Crawford, I., Bower, K. N., Choulaton, T. W., Dearden, C., Crosier, J., Westbrook, C.,
24 Capes, G., Coe, H., Connolly, P. J., Dorsey, J. R., Gallagher, M. W., Williams, P., Trembath,
25 J., Cui, Z. and Blyth, A.: Ice formation and development in aged, wintertime cumulus over
26 the UK: observations and modelling, *Atmos. Chem. Phys.*, 12(11), 4963–4985,
27 doi:10.5194/acp-12-4963-2012, 2012.

28

29 Crawford, I., Gallagher, M. W., Bower, K. N., Choulaton, T. W., Flynn, M. J., Ruske, S.,
30 Listowski, C., Brough, N., Lachlan-Cope, T., Flemming, Z. L., Foot, V. E., and Stanley, W.

1 R.: Real Time Detection of Airborne Bioparticles in Antarctica, *Atmos. Chem. Phys.*
2 *Discuss.*, <https://doi.org/10.5194/acp-2017-421>, in review, 2017.

3 Crosier, J., Bower, K. N., Choularton, T. W., Westbrook, C. D., Connolly, P. J., Cui, Z. Q.,
4 Crawford, I. P., Capes, G. L., Coe, H., Dorsey, J. R., Williams, P. I., Illingworth, A. J.,
5 Gallagher, M. W. and Blyth, A. M.: Observations of ice multiplication in a weakly
6 convective cell embedded in supercooled mid-level stratus, *Atmos. Chem. Phys.*, 11(1), 257–
7 273, doi:10.5194/acp-11-257-2011, 2011.

8 Dee, D. P., Uppala, S. M., Simmons, A. J., Berrisford, P., Poli, P., Kobayashi, S., Andrae, U.,
9 Balmaseda, M. A., Balsamo, G., Bauer, P., Bechtold, P., Beljaars, A. C. M., van de Berg, L.,
10 Bidlot, J., Bormann, N., Delsol, C., Dragani, R., Fuentes, M., Geer, A. J., Haimberger, L.,
11 Healy, S. B., Hersbach, H., Holm, E. V., Isaksen, L., Kållberg, P., Köhler, M., Matricardi, M.,
12 McNally, A. P., Monge-Sanz, B. M., Morcrette, J.-J., Park, B.-K., Peubey, C., de Rosnay, P.,
13 Tavolato, C., Thepaut, J.-N., and Vitart, F.: The ERA-Interim reanalysis: configuration and
14 performance of the data assimilation system, *Q. J. Roy. Meteor. Soc.*, 137, 553–597, 2011.

15 DeMott, P. J., Prenni, a J., Liu, X., Kreidenweis, S. M., Petters, M. D., Twohy, C. H.,
16 Richardson, M. S., Eidhammer, T. and Rogers, D. C.: Predicting global atmospheric ice
17 nuclei distributions and their impacts on climate., *Proc. Natl. Acad. Sci. U. S. A.*, 107(25),
18 11217–22, doi:10.1073/pnas.0910818107, 2010.

19 DeMott, P. J., Hill, T. C. J., McCluskey, C. S., Prather, K. A., Collins, D. B., Sullivan, R. C.,
20 Ruppel, M. J., Mason, R. H., Irish, V. E., Lee, T., Hwang, C. Y., Rhee, T. S., Snider, J. R.,
21 McMeeking, G. R., Dhaniyala, S., Lewis, E. R., Wentzell, J. J. B., Abbatt, J., Lee, C., Sultana,
22 C. M., Ault, A. P., Axson, J. L., Diaz Martinez, M., Venero, I., Santos-Figueroa, G., Stokes,
23 M. D., Deane, G. B., Mayol-Bracero, O. L., Grassian, V. H., Bertram, T. H., Bertram, A. K.,
24 Moffett, B. F. and Franc, G. D.: Sea spray aerosol as a unique source of ice nucleating
25 particles, *Proc. Natl. Acad. Sci.*, 201514034, doi:10.1073/pnas.1514034112, 2015.

26 Dery, S. J. and Yau, M. K.: A climatology of adverse winter-type weather events, *J. Geophys.*
27 *Res.*, 104672(16), 657–16, doi:10.1029/1999JD900158, 1999.

28 Fleming, Z. L., Monks, P. S. and Manning, A. J.: Review: Untangling the influence of air-
29 mass history in interpreting observed atmospheric composition, *Atmos. Res.*, 104–105, 1–39,
30 doi:10.1016/j.atmosres.2011.09.009, 2012.

31 Gallet, J. C., Domine, F., Savarino, J., Dumont, M. and Brun, E.: The growth of sublimation

1 crystals and surface hoar on the Antarctic plateau, *Cryosphere*, 8(4), 1205–1215,
2 doi:10.5194/tc-8-1205-2014, 2014.

3 Geerts, B., Pokharel, B. and Kristovich, D. a. R.: Blowing Snow as a Natural Glaciogenic
4 Cloud Seeding Mechanism, *Mon. Weather Rev.*, 143(12), 5017–5033, doi:10.1175/MWR-D-
5 15-0241.1, 2015.

6 Gibson, J. A. E., Garrick, R. C., Burton, H. R. and McTaggart, A. R.: Dimethylsulfide and the
7 alga *Phaeocystis pouchetii* in antarctic coastal waters, *Mar. Biol.*, 104(2), 339–346,
8 doi:10.1007/BF01313276, 1990.

9 Giordano, M. R., Kalnajs, L. E., Avery, A., Goetz, J. D., Davis, S. M., and DeCarlo, P. F.: A
10 missing source of aerosols in Antarctica – beyond long-range transport, phytoplankton, and
11 photochemistry, *Atmos. Chem. Phys.*, 17, 1-20, doi:10.5194/acp-17-1-2017, 2017.

12 Good, N., Coe, H. and McFiggans, G.: Instrumentational operation and analytical
13 methodology for the reconciliation of aerosol water uptake under sub-and supersaturated
14 conditions, *Atmos. Meas. Tech.*, 3(5), 1241–1254, doi:10.5194/amt-3-1241-2010, 2010.

15 Grosvenor, D. P., Choularton, T. W., Lachlan-Cope, T., Gallagher, M. W., Crosier, J., Bower,
16 K. N., Ladkin, R. S. and Dorsey, J. R.: In-situ aircraft observations of ice concentrations
17 within clouds over the Antarctic Peninsula and Larsen Ice Shelf, *Atmos. Chem. Phys.*, 12(23),
18 11275–11294, doi:10.5194/acp-12-11275-2012, 2012.

19 Hallett, J. and Mossop, S. C. C.: Production of secondary ice particles during the riming
20 process, *Nature*, 249(5452), 26–28, doi:10.1038/249026a0, 1974.

21 Huang, Y., Blyth, A. M., Brown, P. R. A., Choularton, T. W. and Cui, Z.: Factors Controlling
22 Secondary Ice Production in Cumulus Clouds, *Q. J. R. Meteorol. Soc.*, 2017.

23 Jackson, R. C., McFarquhar, G. M., Korolev, A. V., Earle, M. E., Liu, P. S. K., Lawson, R. P.,
24 Brooks, S., Wolde, M., Laskin, A., and Freer, M.: The dependence of ice microphysics on
25 aerosol concentration in arctic mixed-phase stratus clouds during ISDAC and M-PACE, *J.*
26 *Geophys. Res.*, 117, D15207, doi:10.1029/2012JD017668, 2012.

27 Jones, A., Thomson, D., Hort, M. and Devenish, B.: The UK Met Office’s next-generation
28 atmospheric dispersion model, NAME III, *Air Pollut. Model. its ...*, 580–589, 2007.

29 Jones, A. E., Wolff, E. W., Salmon, R. A., Bauguitte, S. J. B., Roscoe, H. K., Anderson, P. S.,
30 Ames, D., Clemitshaw, K. C., Fleming, Z. L., Bloss, W. J., Heard, D. E., Lee, J. D., Read, K.

1 A., Hamer, P., Shallcross, D. E., Jackson, A. V., Walker, S. L., Lewis, A. C., Mills, G. P.,
2 Plane, J. M. C., Saiz-Lopez, A., Sturges, W. T. and Worton, D. R.: Chemistry of the Antarctic
3 Boundary Layer and the Interface with Snow: an overview of the CHABLIS campaign,
4 *Atmos. Chem. Phys.*, 8(14), 3789–3803, doi:10.5194/acp-8-3789-2008, 2008.

5 Junge, K. and Swanson, B. D.: High-resolution ice nucleation spectra of sea-ice bacteria:
6 implications for cloud formation and life in frozen environments, *Biogeosciences Discuss.*, 4,
7 4261–4282, doi:10.5194/bgd-4-4261-2007, 2007.

8 King, J. C., Gadian, A., Kirchgaessner, A., Kuipers Munneke, P., Lachlan-Cope, T. A., Orr,
9 A., Reijmer, C., van den Broeke, M. R., van Wessem, J. M., and Weeks, M.: Validation of the
10 summertime surface energy budget of Larsen C Ice Shelf (Antarctica) as represented in three
11 high-resolution atmospheric models, *J. Geophys. Res.-Atmos.*, 120, 1335–1347,
12 doi:10.1002/2014JD022604, 2015.

13 King, J. C., Lachlan-Cope, T. A., Ladkin, R. S. and Weiss, A.: Airborne measurements in the
14 stable boundary layer over the Larsen Ice Shelf, Antarctica, *Boundary-Layer Meteorol.*,
15 127(3), 413–428, doi:10.1007/s10546-008-9271-4, 2008.

16 Korolev, A. V., Emery, E. F., Strapp, J. W., Cober, S. G., Isaac, G. A., Wasey, M. and
17 Marcotte, D.: Small ice particles in tropospheric clouds: Fact or artifact? Airborne icing
18 instrumentation evaluation experiment, *Bull. Am. Meteorol. Soc.*, 92(8), 967–973,
19 doi:10.1175/2010BAMS3141.1, 2011.

20 Kumai, M.: Identification of Nuclei and Concentrations of Chemical Species in Snow
21 Crystals Sampled at the South Pole, *J. Atmos. Sci.*, 33(5), 833–841, doi:10.1175/1520-
22 0469(1976)033<0833:IONACO>2.0.CO;2, 1976.

23 Lachlan-Cope, T., Listowski, C., and O'Shea, S.: The microphysics of clouds over the
24 Antarctic Peninsula – Part 1: Observations, *Atmos. Chem. Phys.*, 16, 15605-15617,
25 doi:10.5194/acp-16-15605-2016, 2016.

26 Lance, S., Brock, C. A., Rogers, D. and Gordon, J. A.: Water droplet calibration of the Cloud
27 Droplet Probe (CDP) and in-flight performance in liquid, ice and mixed-phase clouds during
28 ARCPAC, *Atmos. Meas. Tech.*, 3(6), 1683–1706, doi:10.5194/amt-3-1683-2010, 2010.

29 Lance, S., Shupe, M. D., Feingold, G., Brock, C. A., Cozic, J., Holloway, J. S., Moore, R. H.,
30 Nenes, A., Schwarz, J. P., Spackman, J. R., Froyd, K. D., Murphy, D. M., Brioude, J.,
31 Cooper, O. R., Stohl, A. and Burkhardt, J. F.: Cloud condensation nuclei as a modulator of ice

1 processes in Arctic mixed-phase clouds, *Atmos. Chem. Phys.*, 11(15), 8003–8015,
2 doi:10.5194/acp-11-8003-2011, 2011.

3 Latham, T. L., Beyersdorf, A. J., Thornhill, K. L., Winstead, E. L., Cubison, M. J., Hecobian,
4 A., Jimenez, J. L., Weber, R. J., Anderson, B. E. and Nenes, A.: Analysis of CCN activity of
5 Arctic aerosol and Canadian biomass burning during summer 2008, *Atmos. Chem. Phys.*,
6 13(5), 2735–2756, doi:10.5194/acp-13-2735-2013, 2013.

7 Lawson, R. P. and Gettelman, A.: Impact of Antarctic mixed-phase clouds on climate, ,
8 111(51), doi:10.1073/pnas.1418197111, 2014.

9 Lawson, R. P., O’Connor, D., Zmarzly, P., Weaver, K., Baker, B., Mo, Q. and Jonsson, H.:
10 The 2D-S (stereo) probe: Design and preliminary tests of a new airborne, high-speed, high-
11 resolution particle imaging probe, *J. Atmos. Ocean. Technol.*, 23(11), 1462–1477,
12 doi:10.1175/JTECH1927.1, 2006.

13 Lawson, R. P., Woods, S. and Morrison, H.: The Microphysics of Ice and Precipitation
14 Development in Tropical Cumulus Clouds, *J. Atmos. Sci.*, 150310071420004,
15 doi:10.1175/JAS-D-14-0274.1, 2015.

16 Legrand, M., Yang, X., Preunkert, S. and Therys, N.: Year-round records of sea salt, gaseous,
17 and particulate inorganic bromine in the atmospheric boundary layer at coastal (Dumont
18 d’Urville) and central (Concordia) East Antarctic sites, *J. Geophys. Res. Atmos.*, 121(2), 997–
19 1023, doi:10.1002/2015JD024066, 2016.

20 Listowski, C. and Lachlan-Cope, T.: The Microphysics of Clouds over the Antarctic
21 Peninsula – Part 2: modelling aspects within Polar WRF, *Atmos. Chem. Phys. Discuss.*,
22 doi:10.5194/acp-2016-1135, in review, 2017.

23 Liu, D., Quennehen, B., Darbyshire, E., Allan, J. D., Williams, P. I., Taylor, J. W., J.-B.
24 Bauguitte, S., Flynn, M. J., Lowe, D., Gallagher, M. W., Bower, K. N., Choulaton, T. W. and
25 Coe, H.: The importance of Asia as a source of black carbon to the European Arctic during
26 springtime 2013, *Atmos. Chem. Phys.*, 15(20), 11537–11555, doi:10.5194/acp-15-11537-
27 2015, 2015.

28 Lloyd, G., Choulaton, T. W., Bower, K. N., Crosier, J., Jones, H., Dorsey, J. R., Gallagher,
29 M. W., Connolly, P., Kirchgassner, A. C. R. and Lachlan-Cope, T.: Observations and
30 comparisons of cloud microphysical properties in spring and summertime Arctic
31 stratocumulus clouds during the ACCACIA campaign, *Atmos. Chem. Phys.*, 15(7), 3719–

1 3737, doi:10.5194/acp-15-3719-2015, 2015a.

2 Lloyd, G., Choullarton, T. W., Bower, K. N., Gallagher, M. W., Connolly, P. J., Flynn, M.,
3 Farrington, R., Crosier, J., Schlenczek, O., Fugal, J. and Henneberger, J.: The origins of ice
4 crystals measured in mixed phase clouds at High-Alpine site Jungfraujoch, *Atmos. Chem.*
5 *Phys. Discuss.*, 15(13), 18181–18224, doi:10.5194/acpd-15-18181-2015, 2015b.

6 Lubin, D., Chen, B., Bromwich, D. H., Somerville, R. C. J., Lee, W. H. and Hines, K. M.:
7 The impact of antarctic cloud radiative properties on a GCM climate simulation, *J. Clim.*,
8 11(3), 447–462, doi:10.1175/1520-0442(1998)011<0447:TIOACR>2.0.CO;2, 1998.

9 Mahesh, A.: Observations of blowing snow at the South Pole, *J. Geophys. Res.*, 108(D22), 1–
10 9, doi:10.1029/2002JD003327, 2003.

11 Mangold, A., Delcloo, A., De Backer, H., Laffineur, Q., Herenz, P., Wex, H., Gossart A.,
12 Souverijns, N., Gorodetskaya I., and Van Lipzig, N.: CCN and aerosol properties at Princess
13 Elisabeth station, East Antarctica, combined with cloud and precipitation observations and air
14 mass origin, *Geophysical Research Abstracts*, EGU2017-18217, EGU General Assembly,
15 Vienna, 2017.

16 Maslanik, J. and J. Stroeve. 1999, updated daily. Near-Real-Time DMSP SSMIS Daily Polar
17 Gridded Sea Ice Concentrations, Version 1. Boulder, Colorado USA. NASA National Snow
18 and Ice Data Center Distributed Active Archive Center. doi:
19 <http://dx.doi.org/10.5067/U8C09DWVX9LM>. [Date Accessed=April 2016].

20 Mauritsen, T., Sedlar, J., Tjernström, M., Leck, C., Martin, M., Shupe, M., Sjogren, S.,
21 Sierau, B., Persson, P. O. G., Brooks, I. M. and Swietlicki, E.: An Arctic CCN-limited cloud-
22 aerosol regime, *Atmos. Chem. Phys.*, 11(1), 165–173, doi:10.5194/acp-11-165-2011, 2011.

23 McFarquhar, G. M. and Cober, S. G.: Single-scattering properties of mixed-phase Arctic
24 clouds at solar wavelengths: Impacts on radiative transfer, *J. Clim.*, 17(19), 3799–3813,
25 doi:10.1175/1520-0442(2004)017<3799:SPOMAC>2.0.CO;2, 2004.

26 McFarquhar, G. M., Zhang, G., Poellot, M. R., Kok, G. L., McCoy, R., Tooman, T., Fridlind,
27 A. and Heymsfield, A. J.: Ice properties of single-layer stratocumulus during the Mixed-Phase
28 Arctic Cloud Experiment: 1. Observations, *J. Geophys. Res. Atmos.*, 112(24), 1–19,
29 doi:10.1029/2007JD008633, 2007.

30 Möhler, O., Field, P. R., Connolly, P., Benz, S., Saathoff, H., Schnaiter, M., Wagner, R.,

1 Cotton, R., Krämer, M., Mangold, A., and Heymsfield, A. J.: Efficiency of the deposition
2 mode ice nucleation on mineral dust particles, *Atmos. Chem. Phys.*, 6, 3007-3021,
3 doi:10.5194/acp-6-3007-2006, 2006.

4 Möhler, O., DeMott, P. J., Vali, G. and Levin, Z.: Microbiology and atmospheric processes:
5 the role of biological particles in cloud physics, *Biogeosciences Discuss.*, 4(4), 2559–2591,
6 doi:10.5194/bgd-4-2559-2007, 2007.

7 Morrison, H., Thompson, G. and Tatarskii, V.: Impact of Cloud Microphysics on the
8 Development of Trailing Stratiform Precipitation in a Simulated Squall Line: Comparison of
9 One- and Two-Moment Schemes, *Mon. Weather Rev.*, 137(3), 991–1007,
10 doi:10.1175/2008MWR2556.1, 2009.

11 Mossop, S. C.: Secondary ice particle production during rime growth: The effect of drop size
12 distribution and rimer velocity, *Q. J. R. Meteorol. Soc.*, 111(470), 1113–1124,
13 doi:10.1002/qj.49711147012, 1985.

14 Mossop, S. C. and Hallett, J.: Ice crystal concentration in cumulus clouds: influence of the
15 drop spectrum., *Science (80-.)*, 186(1963), 632–634, doi:10.1126/science.186.4164.632,
16 1974.

17 Mossop, S. C. C.: Production of secondary ice particles during the growth of graupel by
18 riming, *Nature*, (102), 45–57, doi:10.1038/249026a0, 1976.

19 Murray, B. J., O’Sullivan, D., Atkinson, J. D. and Webb, M. E.: Ice nucleation by particles
20 immersed in supercooled cloud droplets., *Chem. Soc. Rev.*, 41(19), 6519–54,
21 doi:10.1039/c2cs35200a, 2012.

22 Niemand, M., Möhler, O., Vogel, B., Vogel, H., Hoose, C., Connolly, P., Klein, H.,
23 Bingemer, H., DeMott, P., Skrotzki, J. and Leisner, T.: A Particle-Surface-Area-Based
24 Parameterization of Immersion Freezing on Desert Dust Particles, *J. Atmos. Sci.*, 69(10),
25 3077–3092, doi:10.1175/JAS-D-11-0249.1, 2012.

26 Palm, S. P., Yang, Y., Spinhirne, J. D. and Marshak, A.: Satellite remote sensing of blowing
27 snow properties over Antarctica, *J. Geophys. Res. Atmos.*, 116(16), 1–16,
28 doi:10.1029/2011JD015828, 2011.

29 Petters, M. D. and Kreidenweis, S. M.: A single parameter representation of hygroscopic
30 growth and cloud condensation nucleus activity, *Atmos. Chem. Phys.*, (7), 1961–1971,

1 doi:10.5194/acp-13-1081-2013, 2007.

2 Pringle, K. J., Tost, H., Pozzer, A., Pöschl, U., and Lelieveld, J.: Global distribution of the
3 effective aerosol hygroscopicity parameter for CCN activation, *Atmos. Chem. Phys.*, 10,
4 5241-5255, doi:10.5194/acp-10-5241-2010, 2010.

5 Rangno, A. L. and Hobbs, P. V.: Ice particles in stratiform clouds in the Arctic and possible
6 mechanisms for the produc- tion of high ice concentrations, *J. Geophys. Res.*, 106, 15065,
7 doi:10.1029/2000JD900286, 2001.

8 Rosenberg, P. D., Dean, a. R., Williams, P. I., Dorsey, J. R., Minikin, a., Pickering, M. a.
9 and Petzold, a.: Particle sizing calibration with refractive index correction for light scattering
10 optical particle counters and impacts upon PCASP and CDP data collected during the Fenec
11 campaign, *Atmos. Meas. Tech.*, 5(5), 1147–1163, doi:10.5194/amt-5-1147-2012, 2012.

12 Stein, A. F., Draxler, R. R., Rolph, G. D., Stunder, B. J. B., Cohen, M. D., and Ngan, F.:
13 NOAA’s HYSPLIT atmospheric transport and dispersion modeling system, *B. Am. Meteorol.*
14 *Soc.*, 2015, 2059–2077, doi:10.1175/BAMS-D-14-00110.1, 2015.

15 Taylor, J. W., Choulaton, T. W., Blyth, A. M., Liu, Z., Bower, K. N., Crosier, J., Gallagher,
16 M. W., Williams, P. I., Dorsey, J. R., Flynn, M. J., Bennett, L. J., Huang, Y., French, J.,
17 Korolev, A., and Brown, P. R. A.: Observations of cloud microphysics and ice formation
18 during COPE, *Atmos. Chem. Phys.*, 16, 799-826, doi:10.5194/acp-16-799-2016, 2016.

19 Thorpe, A. D. and Mason, B. J.: The evaporation of ice spheres and ice crystals, *Br. J. Appl.*
20 *Phys.*, 17(4), 541, doi:10.1088/0508-3443/17/4/316, 1966.

21 Topping, D. O., Mcfiggans, G. B. and Coe, H.: A curved multi-component aerosol
22 hygroscopicity model framework: Part 1 – Inorganic compounds, , 1205–1222, 2005.

23 Vali, G., Leon, D. and Snider, J. R.: Ground-layer snow clouds, *Q. J. R. Meteorol. Soc.*,
24 138(667), 1507–1525, doi:10.1002/qj.1882, 2012.

25 Verlinde, J., Harrington, J. Y., McFarquhar, G. M., Yannuzzi, V. T., Avramov, A.,
26 Greenberg, S., Johnson, N., Zhang, G., Poellot, M. R., Mather, J. H., Turner, D. D., Eloranta,
27 E. W., Zak, B. D., Prenni, A. J., Daniel, J. S., Kok, G. L., Tobin, D. C., Holz, R., Sassen, K.,
28 Spangenberg, D., Minnis, P., Tooman, T. P., Ivey, M. D., Richardson, S. J., Bahrman, C. P.,
29 Shupe, M., DeMott, P. J., Heymsfield, A. J. and Schofield, R.: The mixed-phase arctic cloud
30 experiment, *Bull. Am. Meteorol. Soc.*, 88(2), 205–221, doi:10.1175/BAMS-88-2-205, 2007.

1 Virkkula, A. and Teinil, K.: Chemical composition of boundary layer aerosol over the
2 Atlantic Ocean and at an Antarctic site, *Atmos. Chem. Phys.*, (January 2000), 3407–3421,
3 2006.

4 Weller, R., Wöltjen, J., Piel, C., Resenberg, R., Wagenbach, D., König-Langlo, G. and
5 Kriews, M.: Seasonal variability of crustal and marine trace elements in the aerosol at
6 Neumayer station, Antarctica, *Tellus, Ser. B Chem. Phys. Meteorol.*, 60 B(5), 742–752,
7 doi:10.1111/j.1600-0889.2008.00372.x, 2008.

8 Weller, R., Minikin, A., Wagenbach, D. and Dreiling, V.: Characterization of the inter-
9 annual, seasonal, and diurnal variations of condensation particle concentrations at Neumayer,
10 Antarctica, *Atmos. Chem. Phys.*, 11(24), 13243–13257, doi:10.5194/acp-11-13243-2011,
11 2011.

12 Whitehead, J. D., Darbyshire, E., Brito, J., Barbosa, H. M. J., Crawford, I., Stern, R.,
13 Gallagher, M. W., Kaye, P. H., Allan, J. D., Coe, H., Artaxo, P. and McFiggans, G.: Biogenic
14 cloud nuclei in the Amazon, *Atmos. Chem. Phys. Discuss.*, (January), 1–23, doi:10.5194/acp-
15 2015-1020, 2016.

16 Wilson, T. W., Ladino, L. A., Alpert, P. A., Breckels, M. N., Brooks, I. M., Browse, J.,
17 Burrows, S. M., Carslaw, K. S., Huffman, J. A., Judd, C., Kilthau, W. P., Mason, R. H.,
18 McFiggans, G., Miller, L. A., Najera, J., Polishchuk, E., Rae, S., Schiller, C. L., Si, M.,
19 Vergara Temprado, J., Whale, T. F., Wong, J. P. S., Wurl, O., Yakobi-Hancock, J. D., Abbott,
20 J. P. D., Aller, J. Y., Bertram, A. K., Knopf, D. A. and Murray, B. J.: A marine biogenic
21 source of atmospheric ice nucleating particles, *Nature*, doi:10.1038/nature14986, 2015.

22 Xu, L., Russell, L. M., Somerville, R. C. J., and Quinn, P. K.: Frost flower aerosol effects on
23 Arctic wintertime longwave cloud radiative forcing, *J. Geophys. Res.-Atmos.*, 118, 13282–
24 13291, doi:10.1002/2013JD020554, 2013.

25 Yang, X., Pyle, J. A. and Cox, R. A.: Sea salt aerosol production and bromine release: Role of
26 snow on sea ice, *Geophys. Res. Lett.*, 35(16), 1–5, doi:10.1029/2008GL034536, 2008.

27 Yano, J.-I. and Phillips, V. T. J.: Ice–Ice Collisions: An Ice Multiplication Process in
28 Atmospheric Clouds, *J. Atmos. Sci.*, 68(2), 322–333, doi:10.1175/2010JAS3607.1, 2011.

29